Geophysical Journal International

Geophys. J. Int. (2015) **200,** 421–438 doi: 10.1093/gji/ggu404
GJI Seismology

New predictive equations and site amplification estimates for the next-generation Swiss ShakeMaps

Carlo Cauzzi,[1] Benjamin Edwards,[1] Donat Fäh,[1] John Clinton,[1] Stefan Wiemer,[1] Philipp Kästli,[1] Georgia Cua[2,*] and Domenico Giardini[3]

[1] *Swiss Seismological Service (SED) at ETHZ, Sonneggstrasse* 5, 8092 *Zürich, Switzerland. E-mail: carlo.cauzzi@sed.ethz.ch*
[2] *Independent Engineering Seismology Consultant*
[3] *Institute of Geophysics at ETHZ, Sonneggstrasse* 5, 8092 *Zürich, Switzerland*

Accepted 2014 October 14. Received 2014 October 7; in original form 2014 June 20

SUMMARY

We present a comprehensive scientific and technical update of the Swiss customization of United States Geological Survey *ShakeMap*, in use at the Swiss Seismological Service since 2007. The new Swiss *ShakeMaps* are based on predictive equations for peak ground-motions and response spectra derived from stochastic simulations tailored to Swiss seismicity. Using synthetics allows overcoming the difficulties posed by: (i) the paucity of strong-motion data recordings in Switzerland; (ii) the regional dependence of shear wave energy attenuation and focal depth distribution in the Swiss Alps and foreland; (iii) the depth dependence of stress parameters suggested by macroseismic and instrumental observations. In the new Swiss *ShakeMaps*, $V_{S,30}$ is no longer used as proxy for site amplification at regional scale, and is replaced by macroseismic intensity increments for different soil classes, based on the recently revised earthquake catalogue of Switzerland (ECOS-09). The new implementation converts ground-motion levels into macroseismic intensity by means of ground-motion to intensity conversion equations based on the Italian strong-motion and intensity databanks and is therefore well constrained for intensities larger than VII. The new Swiss *ShakeMaps* show a satisfactory agreement with the macroseimic fields of both large historical events and recent well-recorded earthquakes of moderate magnitude. The new implementation is now fully consistent with the state-of-the-art in engineering seismology in Switzerland.

Key words: Earthquake ground motions; Seismic attenuation; Site effects; Computational seismology; Early warning.

1 INTRODUCTION AND MOTIVATION

ShakeMap is a well-known scientific and technical framework that provides near real time (i.e. within minutes of an earthquake origin time) seismic shaking scenarios based on recorded and predicted ground-motions [peak ground acceleration (*PGA*) and peak ground velocity (*PGV*)], 5 per cent-damped pseudo-acceleration spectral ordinates (*PSA*) and macroseismic intensity (*I*) levels, including amplification due to local site effects. *ShakeMap* was first developed for significant earthquakes in California (Wald *et al.* 1999) and is nowadays routinely used in many other regions in the United States and worldwide in order to optimize emergency response capabilities and information dissemination following relevant earthquake events.

In Switzerland, the *ShakeMap* codes (Wald *et al.* 2005) distributed by the United States Geological Survey (USGS) have been used since 2007 at the Swiss Seismological Service (SED, http://www.seismo.ethz.ch, last accessed 3 November 2014) to provide national-scale maps of the spatial variability of ground-motions and EMS-98 macroseismic intensity (Grünthal 1998; Grünthal & Levret 2001) following any local earthquake with local magnitude $M_L \geq 2.5$ located in the greater Swiss region.

The first customization of the *ShakeMap* codes (version 3.2) for Swiss conditions, carried out in 2007, required: (i) developing ground-motion prediction equations (GMPEs) for *PGA* and *PGV* based on Swiss earthquake recordings, augmented with the NGA-West1 (Chiou *et al.* 2008) data set to improve the reliability of the predictive tool at moderate and large magnitudes (Cua & Heaton 2008; hereafter CH08); (ii) computing a uniformly spaced grid of 'pseudo-$V_{S,30}$' values inferred from a data set of observed macroseismic intensity amplification values (Kästli & Fäh 2006; Cua *et al.* 2007) with respect to median intensity predictions for Switzerland (Fäh *et al.* 2003); (iii) adopting the Swiss specific ground-motion to intensity conversion equation (GMICE) of Kästli & Fäh (2006, henceforth KF06), used by *ShakeMap* to convert *PGV* observations into EMS-98 intensity levels.

*Formerly at: Swiss Seismological Service (SED) at ETHZ, Sonneggstrasse 5, 8092 Zürich, Switzerland.

Since late 2012, following a migration to the earthquake monitoring software SeisComP3 (Hanka *et al.* 2010; http://www.seiscomp3.org, last accessed 3 November 2014) at the SED, the peak-motion parametric data that are used as input to *ShakeMap* are automatically computed by the software module *scwfparam* (Cauzzi *et al.* 2013) once a new SeisComP3 earthquake origin is available. This means that all seismic stations that are used in real-time by the SED for earthquake detection, location and further characterization also now contribute to the production of SED *ShakeMaps*. The SED presently (2014 September) acquires data in real-time from 83 broad-band velocity sensors, 28 short-period velocity sensors and 85 broad-band acceleration sensors, all recording on 24-bit digitizers, from across Switzerland and neighbouring regions. The module *scwfparam* also allows automatic updates when a manual revision of the earthquake magnitude and location is available, as well as playback reprocessing. An overview of the Swiss national seismic monitoring networks can be found at http://www.seismo.ethz.ch/monitor/net_maps/index_EN (last accessed 3 November 2014). A detailed description of the strong-motion station subset, critical for *ShakeMap*, is described by Clinton *et al.* (2011) and Cauzzi & Clinton (2013). The SED *ShakeMaps* described above, referred to as *SEDShakeMap32* (as they are developed for version 3.2), are automatically generated and posted to public webpages within approximately 5 min of the earthquake origin time. A website is devoted to hosting the USGS-style *ShakeMaps* and related metadata (http://sedshakemap.ethz.ch, last accessed 3 November 2014), while the spatial grid of peak-motion values and intensity data produced by *ShakeMap* is automatically parsed by an *ad hoc* developed Java code and subsequently used by the SED Web-mapping application programming interface (see http://www.seismo.ethz.ch/eq/latest/index?time=utc, last accessed 3 November 2014).

The recently completed Pegasos Refinement Project (PRP, http://www.swissnuclear.ch/en/pegasos-verfeinert.html, last accessed 3 November 2014) focused on updating and improving probabilistic seismic hazard analyses for Swiss nuclear power plants. The research efforts carried out within the project between 2008 and 2013 resulted in a variety of important scientific results with immediate applications in Switzerland, concerning in particular an improved definition of seismic shaking levels and site effects throughout the country (e.g. Fäh *et al.* 2011; Poggi *et al.* 2011; Edwards & Fäh 2013). In-parallel to PRP, the first phase of the upgrade project of the Swiss strong-motion network (SSMNet; Clinton *et al.* 2011; Cauzzi & Clinton 2013) improved the quality and quantity of the strong motion data being recorded across the nation and also included detailed geophysical characterization at a majority of new and existing Swiss strong-motion stations (Edwards *et al.* 2013; Michel *et al.* 2014).

Spurred by these developments in the PRP and the SSMNet renewal project, a careful revision of the scientific and technical basis of the Swiss *ShakeMaps* has been undertaken during the last 15 months. In particular, it was considered important to migrate the state-of-the-art tools used in hazard assessment into standard seismic network products. Amongst the changes and improvements implemented in Swiss *ShakeMaps* are:

(1) The parametrization of the stochastic ground-motion predictions at hard rock sites by Edwards & Fäh (2013), EF13, allowing the prediction of response spectra in addition to *PGA* and *PGV*.

(2) The use of the GMICE by Faenza & Michelini (2010), FM10.

(3) The verification of the regional amplification factors based on macroseismic intensity data (Kästli & Fäh 2006; Fäh *et al.* 2011).

(4) The comparison of the new intensity predictions with the recently recompiled earthquake catalogue of Switzerland ECOS-09 (Fäh *et al.* 2011).

Furthermore, in order to take full advantage of the major improvements in the latest USGS code, SED is currently transitioning to *ShakeMap* version 3.5. One new feature is the implementation of region-specific predictive equations, critical in the Swiss context, where the attenuation of shear wave energy is regionally dependent (Edwards *et al.* 2011) and the earthquakes located in the alpine region typically occur at shallower depths than those located in the Swiss foreland (Fäh *et al.* 2011; Diehl *et al.* 2013, 2014).

In this contribution, we present and discuss the main elements of the scientific background of the new Swiss *ShakeMaps*, hereafter referred to as *SEDShakeMap35* (as they are developed for version 3.5). The functional parametrization of ground-motions and response spectra predicted by EF13 is first introduced and compared with the recordings of recent local earthquakes. The ground-motion to intensity conversions of FM10 are then compared with KF06 and used to translate the ECOS-09 macroseismic intensity amplification map into a map of *PGV* amplification for *ShakeMap*. The intensity predictions obtained using EF13, FM10 and the aforementioned intensity amplification data are then combined and used to perform a residual analysis based on the historical macroseismic intensity catalogue of Switzerland for events with moment magnitude $M_W \geq 4.7$. Finally, a selection of historical and instrumental earthquake shaking scenarios obtained from *SEDShakeMap35* and *SEDShakeMap32* is presented and discussed. The Appendix is aimed at providing the reader with additional useful information as to the behaviour of the Swiss stochastic ground-motion prediction model through the comparison with popular empirical predictive equations in use in Switzerland and in Europe, namely: the previously adopted model Cua & Heaton (2008), CH08, the recently published Pan-European predictive equations of Akkar *et al.* (2014), ASB14 and the global broad-band prediction model of Cauzzi & Faccioli (2008), CF08.

2 PREDICTIVE EQUATIONS FOR *PGA*, *PGV* AND *PSA* (*T; 5 per cent*)

Edwards & Fäh (2013) formulated a stochastic ground-motion model for Switzerland (EF13) based on a typical earthquake scenario, path effects (Edwards *et al.* 2011) and site amplification referenced to a known velocity model (Poggi *et al.* 2011). The model was calibrated against recorded weak-motion data for frequencies $f \geq 0.5$ Hz and its validity extended through calibration at high magnitudes with the Swiss macroseismic intensity attenuation model used to determine historical earthquake magnitudes (Fäh *et al.* 2011). The use of the effective distance in the EF13 model facilitates the simulation of average geometric finite-fault effects for random hypocentre and slip (Atkinson *et al.* 2009; Boore 2009), that is, modelling of features such as the saturation of near-field ground motion with increasing magnitude and the magnitude dependence of the geometrical decay with distance.

ShakeMap is just one of the many potential applications of EF13 where the direct stochastic simulation of shaking levels is inefficient (others being, for example, early warning and probabilistic seismic hazard analyses), and where a functional form of the stochastic model would be preferable. In *ShakeMap*, the ground motions at 'phantom' stations (gridpoints where no direct measurement of peak motions is available) are indeed estimated using a ground-motion prediction equation (GMPE) suitable for the region of interest.

A finite source distance model is therefore presented here, based on the distance from the ruptured fault R_{RUP}, which is approximately equal to the focal (hypocentral) distance R for moment magnitude $M_{\mathrm{W}} < 5.7$ (see e.g. Faccioli *et al.* 2010 and Cauzzi *et al.* 2014). The predictive equations derived here replicate the average synthetic prediction evenly spanning the magnitude range 2–8 and distance range 0–340 km. The reference rock condition corresponds to a $V_{\mathrm{S},30}$ of 1105 m s^{-1} (Poggi *et al.* 2011). For each spectral period, *PGA* and *PGV*, the data set consists of approximately 400 000 records from 1200 simulated earthquakes. The depth distribution of the events in the synthetic data set is based on the manual Swiss earthquake catalogue comprising more than 2200 regional events with $M_{\mathrm{L}} \geq 2$ that occurred between 1975 and 2008 (Deichmann 2010; Fäh *et al.* 2011). For the Swiss alpine region, 43 per cent of the simulated events have depths of less than 3 km, 49 per cent between 3 and 7 km, while 8 per cent are located at greater depths. For the Swiss foreland, 25 per cent of the events are located at less than 4 km depth, 39 per cent between 4 and 10 km, 21 per cent between 10 and 17 km and 15 per cent at greater depths. Consistent with many other ground-motion prediction studies in Europe and worldwide (e.g. Douglas *et al.* 2014), the output of our simulations is the common geometric mean of the horizontal components of ground motions.

Investigations aimed at identifying the preferred functional forms of the predictive equations were initially carried out on a set of simulations corresponding to a maximum stress parameter (stress-drop) value $\Delta\sigma = 60$ bar, as recommended by Edwards & Fäh (2013). The chosen functional form was then also used to fit synthetic data generated by simulations with different values of the maximum stress-drop (ranging from 10 to 120 bar). Simulations with maximum $\Delta\sigma$ values significantly different from the recommended 60 bar were included in the data set in order to test their ability to reproduce the macroseismic fields of the largest historical events in the earthquake catalogue of Switzerland, as described later in Section 5.

The predictive equations for *PGA*, *PGV* and *PSA* (T; 5 per cent) take the form:

$$\log_{10} y = f_M + f_d + \varepsilon, \tag{1}$$

where

$$f_M = m_0 + m_1 M_{\mathrm{W}} + m_2 M_{\mathrm{W}}^2 + m_3 M_{\mathrm{W}}^3 + m_4 M_{\mathrm{W}}^4 + m_5 M_{\mathrm{W}}^5 + m_6 M_{\mathrm{W}}^6 \tag{2}$$

$$f_d = \left(r_1 + r_2 M_{\mathrm{W}} + r_3 M_{\mathrm{W}}^2 + r_4 M_{\mathrm{W}}^3\right) d + \left(r_5 + r_6 M_{\mathrm{W}} + r_7 M_{\mathrm{W}}^2 + r_8 M_{\mathrm{W}}^3\right) d^2 + \left(r_9 + r_{10} M_{\mathrm{W}} + r_{11} M_{\mathrm{W}}^2 + r_{12} M_{\mathrm{W}}^3\right) d^3 + \left(r_{13} + r_{14} M_{\mathrm{W}} + r_{15} M_{\mathrm{W}}^2 + r_{16} M_{\mathrm{W}}^3\right) d^4 \tag{3}$$

and

$$d = \log_{10} \left\{ \max \left[R_{RUP}, r_{\min}(M_{\mathrm{W}}) \right] \right\}. \tag{4}$$

M_{W} is the moment magnitude and $m_{0\ldots6}$, $r_{1\ldots16}$ are period dependent coefficients determined through regressions on the synthetic data. y can be *PGV* in cm s^{-1}, *PGA* in cm s^{-2} or *PSA* (T; $\zeta =$ 5 per cent) in cm s^{-2}, where T is the vibration period, in s. ε is a random error term assumed to be normally distributed with zero mean and standard deviation $\sigma(\log_{10} y)$. Aimed at highly accurate reproduction of the synthetic data, the functional form uses high-order polynomials rather than piecewise linear approximations of ground-motion scaling and attenuation to avoid singularities in the distribution of the residuals. The magnitude scaling of the synthetic data was modelled as a 6th order polynomial in the variable M_{W}. As to the distance dependence, a 4th order polynomial in the variable d was found to satisfactorily reproduce the different branches of the distance decay modelled by EF13 in the Swiss alpine and foreland region, including the geometric and anelastic attenuation, as well as the Moho bounce (Burger *et al.* 1987). The distance decay in EF13 is consistent with the findings of Edwards *et al.* (2011), who modelled the apparent geometrical spreading function $S(t)$ as a piecewise three-part function comprising segments of constant exponential decay: this parametrization allows inclusion of Moho reflection phases in the spectrum in the range of 20–140 km in the Swiss Foreland and from 70 to 140 km in the Swiss Alps (see also Bay *et al.* 2003).

Including the distance cut-off term $r_{\min}$ at the beginning of the regressions resulted in a prediction model that is linear in the parameters, meaning less computational time and increased stability of the regressions. Although three main different faulting mechanisms (strike-slip, normal and reverse) were modelled in the synthetic data set, style-of-faulting terms were not explicitly introduced in the predictive model due to their negligible impact on the simulated ground-motions used in this study. Note that while the functional form applies to both the Swiss alpine and the foreland regions, the values of the period-dependent coefficients as well as the formula for computing $r_{\min}(M_{\mathrm{W}})$ are regionally dependent:

$$r_{\min}(Alps) = \begin{cases} 0.55 & \text{if } M_{\mathrm{W}} \geq 5 \\ -2.8 M_{\mathrm{W}} + 14.55 & \text{if } 4.7 \leq M_{\mathrm{W}} < 5 \\ -0.295 M_{\mathrm{W}} + 2.65 & \text{if } M_{\mathrm{W}} < 4.7 \end{cases}. \tag{5}$$

$$r_{\min}(Foreland) = \begin{cases} 0.55 & \text{if } M_{\mathrm{W}} \geq 5.5 \\ -2.067 M_{\mathrm{W}} + 11.92 & \text{if } 4.7 \leq M_{\mathrm{W}} < 5.5 \\ -0.291 M_{\mathrm{W}} + 3.48 & \text{if } M_{\mathrm{W}} < 4.7 \end{cases}. \tag{6}$$

The coefficients of the predictive equations were separately derived for both the Swiss alpine and foreland regions, and are available as Supporting Information, along with *Matlab* scripts for the implementation of eq. (1). The standard deviation of the residuals of eq. (1), $\sigma(\log_{10} y)$, typically range between 0.035 and 0.055. While these values represent the overall goodness of fit of the predictive model with respect to the synthetic data set, implementation of the GMPE should make use of the single station *sigma* σ_{SS} values given in table 5 of Edwards & Fäh (2013).

Fig. 1 shows the median predictions of *PGA* (top panels) and *PGV* (bottom panels) computed using eq. (1), as a function of rupture distance $1 \leq R_{\mathrm{RUP}} \leq 200$ km, for Swiss scenario events with moment magnitude $3 \leq M_{\mathrm{W}} \leq 7$. LHS panels show the predictions for alpine events, while foreland events are depicted in the RHS panels. Apparent from Fig. 1 are the main physical features of the predictive model, that is the saturation of peak ground-motions with distance and magnitude, and the magnitude-dependence of the attenuation with distance. As expected, magnitude saturation is more pronounced at high frequencies (*PGA*) rather than at intermediate periods (*PGV*). Indeed, a slight oversaturation (e.g. Boore *et al.* 2014; Cauzzi *et al.* 2014) of near-source *PGA* values can be observed for $M_{\mathrm{W}} > 6$.

A comparison of eq. (1) with recorded peak ground-motion data generated by two recent events extracted from the instrumental

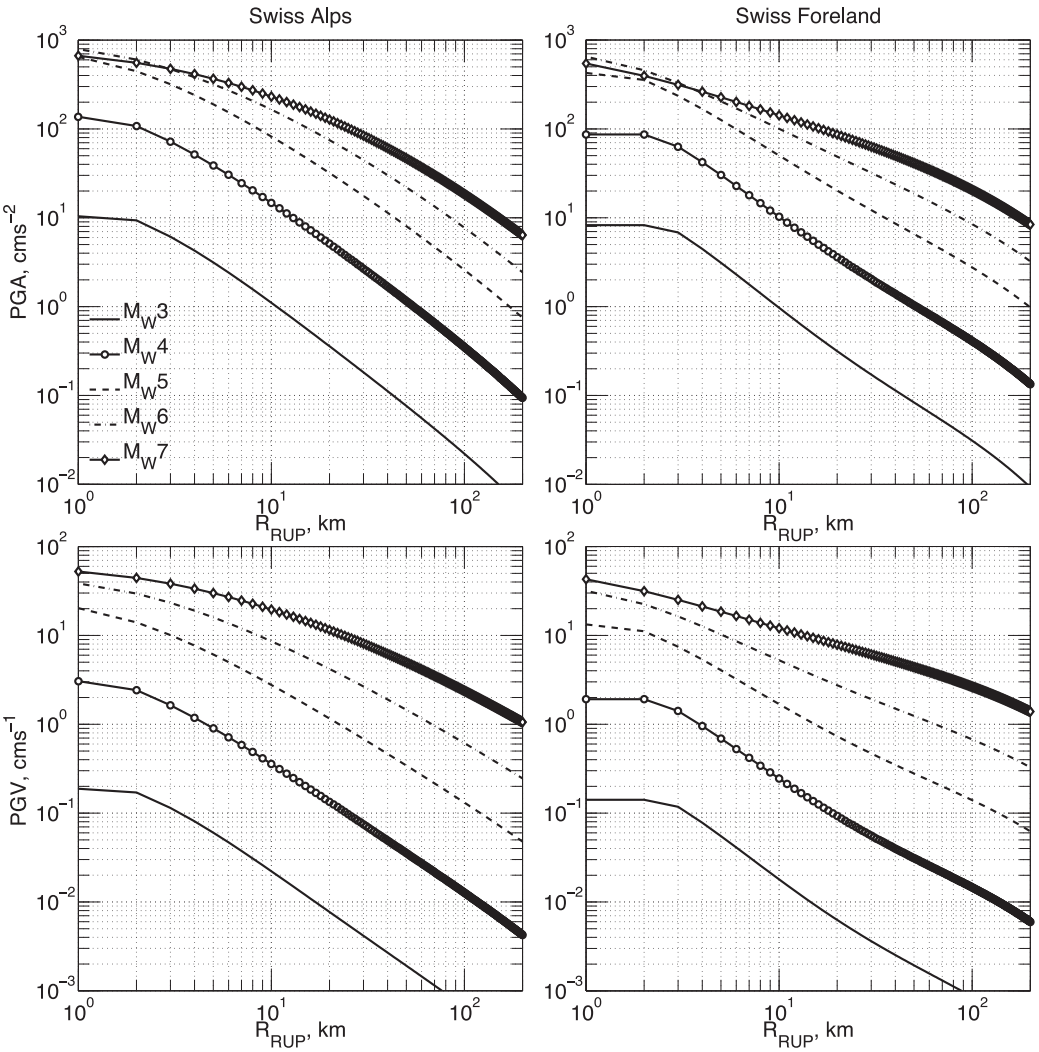

Figure 1. *PGA* (top panels) and *PGV* (bottom panels) predictions based on EF13 ($\Delta\sigma = 60$ bar) as a function of moment magnitude $3 \leq M_W \leq 7$ and rupture distance $1 \leq R_{RUP} \leq 200$ km, in the Swiss alpine (left-hand side) and foreland (right-hand side) region.

catalogue of Switzerland is shown in Fig. 2. The chosen earthquakes are characterized by comparable magnitude and remarkably different depths, namely the M_L 4.2 2012 Zug event (central Switzerland, foreland region, depth ∼32 km; Diehl *et al.* 2013) and the M_L 4.1 2013 Balzers earthquake (eastern Switzerland, alpine region, depth ∼7 km; Diehl *et al.* 2014). Both the Zug and the Balzers event were clearly recorded by the seismic stations continuously streaming data in real-time to the SED. The *PGA* and *PGV* values (geometric mean of the two as-recorded horizontal components) are shown in Fig. 2 as a function of the hypocentral distance. LHS panels refer to the Zug 2012 event, RHS panels to the Balzers 2013 event. Peak ground-motions were computed using *scwfparam* after restitution and zero-phase bandpass filtering (3 s–80 per cent of the Nyquist frequency) of the recorded time-histories. Depicted as grey curves are also the EF13 predictions (median values $\pm 1\sigma$), as implemented in *ShakeMap35*. Since data were not segregated into different soil classes or ground types, the hard-rock EF13 predictions were modified to take into account an average amplification to generic rock-like conditions, as described later in Section 4. In particular, $\log_{10}PGA$ values were incremented by 0.47/2.58 and $\log_{10}PGV$ observations by 0.47/2.35, where 2.58 and 2.35 are the mean values of the slope of the GMICE of Faenza and Michelini (2010) for *PGA* and *PGV*, respectively. For both events, *PGA* exceeded 1 per cent g at the stations closest to the epicenter, while the maximum peak ground velocity *PGV* was ∼0.2 cm s^{-1} for the Zug event and ∼0.4 cm s^{-1} for the Balzers earthquake. Despite the large dispersion of peak-motion data, mainly due to sharp variations in geological and geotechnical features at the recording sites, the predictive models show a satisfactory agreement with the recorded data, in particular to the rate of attenuation with distance for the shallower Balzers event. The comparison is less satisfactory for the deep Zug event that, in spite of a comparable magnitude, exhibited considerably higher ground-motions over a broad distance range, along with a stronger attenuation with distance. The reason can be found in the geometrical spreading term in EF13, which models the supercritical SMS reflection from the Moho independent of source depth. However, deep events provide more reflected energy at close distance because reflected SMS are observed closer to the source than the model predicts. Using the same reasoning, for this deep event near the Moho, at larger distances the expected energy from the SMS bounce as expected in the model will be absent. Overall, the results depicted in Fig. 2 show that eq. (1) can adequately predict peak ground-motion values from Swiss earthquakes, even if not included in the original calibration database of EF13.

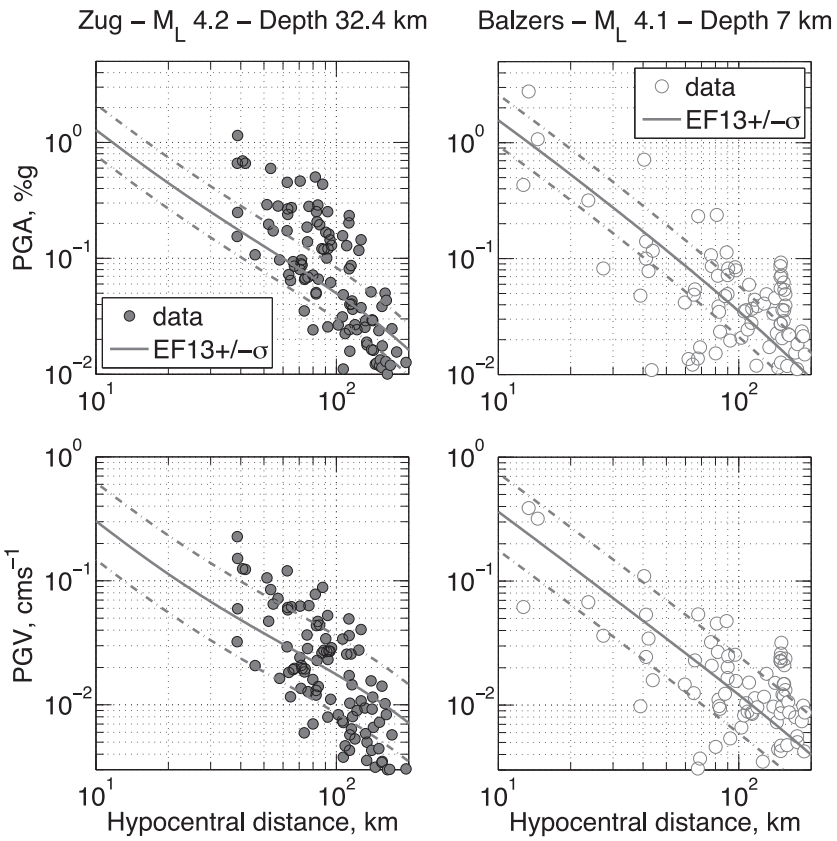

Figure 2. *PGA* (top panels) and *PGV* (bottom panels) data variation as a function of focal distance, as recorded by the real-time stations monitored by the SED. Left-hand side: Zug 2012 event. Right-hand side: Balzers 2013 event. Superimposed on the peak-motion data are the predictions of EF13 (median values $\pm 1\sigma$) as implemented in *SEDShakeMap35*.

3 GROUND-MOTION TO INTENSITY CONVERSION EQUATIONS (GMICEs)

As mentioned in the introduction, *ShakeMap* converts available peak ground velocity (*PGV*) recordings and predictions into macroseismic intensity, by means of a ground motion to intensity prediction equation (GMICE) suitable for the region of interest. In *SEDShakeMap35*, the GMICE of Faenza & Michelini (2010), FM10, is implemented. This is consistent with the approach of PRP, and replaces the Swiss specific GMICE of Kästli & Fäh (2006), KF06, which was used in previous *ShakeMap* implementations. The FM10 conversion of *PGV* into intensity is given by:

$$I_{\mathrm{MCS}} = 5.11 + 2.35 \log_{10} PGV \left(\mathrm{cm\ s^{-1}}\right), \ \sigma = 0.26, \qquad (7)$$

where σ is the standard deviation of the regression. FM10 is a based on a data set of peak ground-motions and associated MCS-intensity data coming from the Italian database of macroseismic information, DBMI04 (http://emidius.mi.ingv.it/DBMI04/, last accessed 3 November 2013) and the ITalian ACcelerometric Archive, ITACA (http://itaca.mi.ingv.it, last accessed 3 November 2014, Pacor *et al.* 2011). The main advantage of using FM10 instead of KF06 is that the calibration data set of the former contains ground motion recordings associated to observed intensities higher than VII. Additionally, the same data set was used to develop GMICEs for *PGA* and spectral ordinates at 0.3, 1 and 2 s (Faenza & Michelini 2011). Furthermore, FM10 was developed using the orthogonal distance regression technique: this means that eq. (7) can be used either to predict intensity from *PGV* or to predict *PGV* from intensity, and the same standard deviation applies in both directions. The reader is referred to

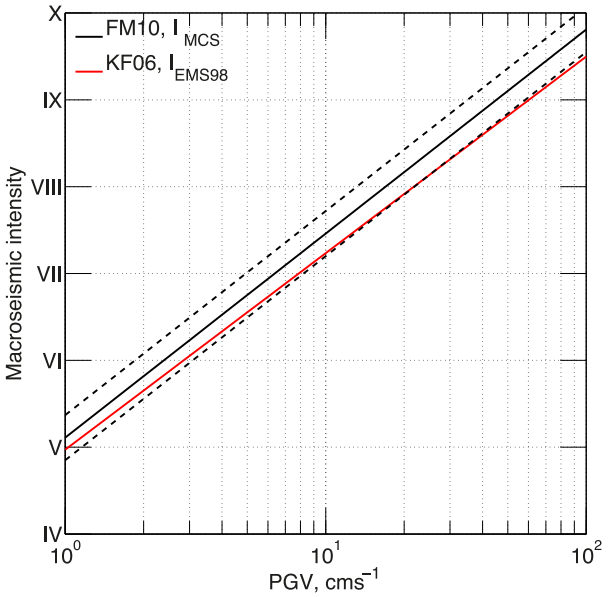

Figure 3. Comparison of the GMICEs for *PGV* by KF06 and FM10. Solid lines: mean values. Dashed lines: $\pm 1\sigma$ bounds of FM10.

Faenza & Michelini (2010) for a comprehensive discussion on (i) the importance of using a biunique regression (i.e. correspondence between the two sets of data is one-to-one along both directions); (ii) the specific definition of the uncertainties for both variables and (iii) the data binning before processing the data. Eq. (7) and the mean values of KF06 are shown in Fig. 3. As apparent from

the figure, we cannot reject the hypothesis that KF06 is equivalent, at least in a statistical sense, to FM10, as the mean prediction of KF06 is always within the -1σ bound of the mean values of FM10. Beyond the aforementioned differences in the strong-motion data sets used for the analyses, the minor differences between the two GMICEs can be most likely attributed to the different vulnerability of the building stock in Switzerland and in Italy. Note that according to Musson *et al.* (2009), no empirical conversion is necessary between the EMS-98 and the MCS intensity scales. Therefore, in the following sections, the word 'intensity' refers to the degrees of the EMS-98 scale, even if intensity levels are derived from *PGV* using FM10. Using a ground-motion to intensity conversion like eq. (7) implies computing the instrumental intensity as a continuous variable, while observed macroseimic intensity is discrete and ordinal by definition. The $\pm 1\sigma$ bounds of eq. (7), roughly equal to 1/2 a degree in intensity, can be used to define a practical strategy to compare instrumental and observed intensities, where necessary: for example, instrumental intensity values in the range I(integer) $\pm$ 0.25 can be assumed to be representative of intensity degree I(ordinal); instrumental intensity values in the range I (integer) + 0.5 $\pm$ 0.25 would then map into (uncertain) intensity assessments like degree $I - (I+1)$ (ordinal).

4 SITE EFFECTS

A significant development during PRP and the first phase of the SSMNet upgrade project is the assessment of site-specific broad-band amplification functions with respect to EF13 and the consequent ability to estimation of $V_{S,30}$ for the majority of the Swiss real-time seismic stations (Cauzzi & Clinton 2013; Edwards *et al.*, 2013; Michel *et al.* 2014). However, at national or regional level, that is for all those sites where a seismic monitoring station is not available, the most reliable and physically sound proxy for amplification phenomena is presently given by mapping changes in the average macroseismic intensity ΔI (Kästli & Fäh 2006; appendix D-1 of Fäh *et al.* 2011) with respect to the mean values of the Swiss intensity prediction equation (IPE) of Fäh *et al.* (2011). Following Fäh (1985), these intensity increments were determined based on soil classes, after careful scrutiny of the differences between observed intensities and those estimated through the Swiss IPE. A prerequisite for the application of this method is a long track record (over centuries) of macroseismic intensities that have been consistently assigned, as available for Switzerland. The intensity amplification increments typically range between –1/4 (in the Swiss Alps) and +1 intensity units (in the region of Basel and in the Swiss alluvium-filled alpine basins). The amplification is actually unknown, and therefore assumed equal to zero in the present study, for large areas in Germany and France, as well as in the Swiss Alps. The macroseismic intensity increments (sampled on a regular grid with Δ_latitute $= \Delta$_longitude $= 0.0135^{\circ}$) are shown in the top panel of Fig. 4. Consistent with PRP, the mapped values include a constant correction term $\Delta I_{\rm rock} \sim +1/2$ intensity units (namely 0.47) that accounts for the necessary adjustment from the hard-rock prediction ($V_{S,30} \sim 1105$ m s^{-1}) of EF13 to the generic rock-like soil class of the Swiss IPE.

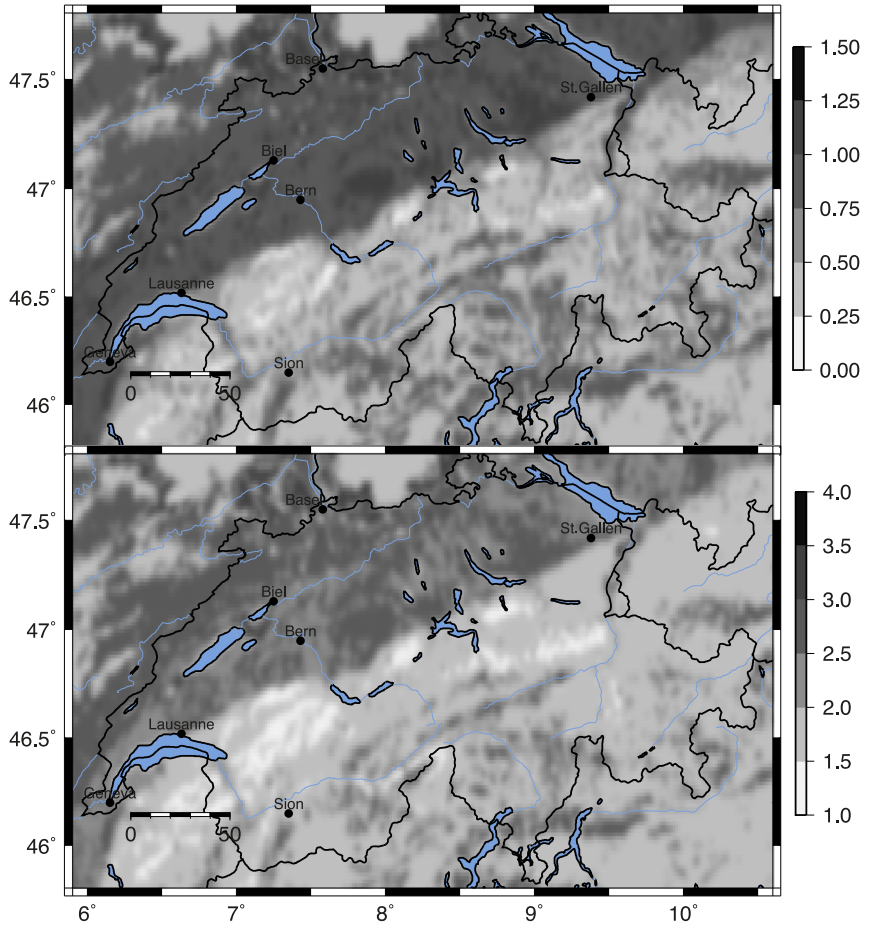

Figure 4. Top panel: regional macroseimic intensity amplification increments $\Delta I_{\rm site}$ computed following Fäh *et al.* (2011). National administrative boundaries are shown as black curves. Bottom panel: multiplicative amplification factors obtained after conversion of $\Delta I_{\rm site}$ into $\Delta \log_{10} PGV$ based on eq. (8).

As previously mentioned, eq. (7) can be inverted to transform the intensity increments $\Delta I_{\rm site} = \Delta I + \Delta I_{\rm rock}$ shown in Fig. 4 (top panel) into a map of *PGV* amplification, as follows:

$$\Delta \log_{10} PGV = (1/2.35)(\Delta I + \Delta I_{\rm rock}). \quad (8)$$

Eq. (8) is directly added to eq. (1) as a site term for *PGV* predictions and the same approach can be adopted for *PGA* and *PSA* (*T*; 5 per cent). Eq. (8) corresponds to the multiplicative amplification factors for *PGV* shown in the bottom panel of Fig. 4. The maximum amplification approaches ∼3.5 in the alluvium-filled alpine valleys and in parts of the Swiss Foreland. The minimum amplification is ∼1.2 in some areas in the northern Alps. Note that the geological boundary between the Swiss alpine and foreland region (modelled in *SEDShakeMap35* as a straight line connecting the cities of Lausanne, in the southwest, and Sankt Gallen, in the northeast) is well marked by a relatively sharp discontinuity in the amplification levels. At a seismic station level, following Edwards *et al.* (2013), the soil class amplification factors are substituted by the actual recorded amplification with respect to the Swiss reference rock model of Poggi *et al.* (2011).

5 CHECKING THE PREDICTIONS AGAINST MACROSEISMIC INTENSITY DATA

In this section, we compare the intensity estimates obtained using EF13, FM10 and the site effect corrections described previously with the macroseismic intensity data points (IDPs) of the most relevant historical events listed in the recently revised earthquake catalogue of Switzerland ECOS-09 (Fäh *et al.* 2011). As mentioned in Section 2, the parametrization of EF13 was performed based on synthetic data sets characterized by different values of the maximum stress-drop $\Delta\sigma$, namely 10, 20, 30, 50, 60, 75, 90 and 120 bar. Simulations with maximum $\Delta\sigma$ values different from 60 bar (recommended by EF13) were taken into account to check their ability to reproduce the macroseismic fields of the historical earthquakes. The goal of this investigation is to rank different $\Delta\sigma$ models in order to select the optimal implementation for *SEDShakeMap35*, following a simplified logic-tree approach.

The catalogue earthquakes used for the analyses are listed in Table 1. The distribution of magnitude, epicentral distance and epicentral region (Swiss Alps and Foreland) for the macroseismic data set is shown in Fig. 5. The data set comprises ∼2000 datapoints from 23 earthquakes, with moment magnitude $M_{\rm W}$ in the range 4.7–6.6 and maximum epicentral distance of ∼230 km. Depth is known, albeit with large uncertainties, for only ∼50 per cent of the historical earthquakes. The epicentral location of the historical events is also associated with large uncertainties and, with the exception of a few well-documented cases (e.g. Fritsche *et al.* 2006; Fäh *et al.* 2009), little or no information is available about the causative faults

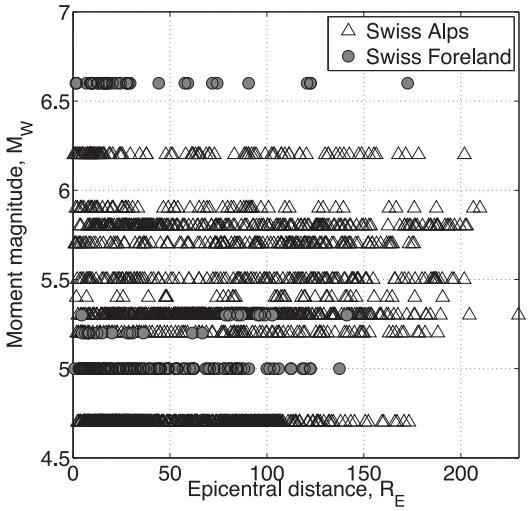

Figure 5. Distribution of magnitude, epicentral distance and epicentral region for the intensity datapoints (IDPs) used in this study.

Table 1. Excerpt of the earthquake catalogue of Switzerland (ECOS-09), listing historical events with $M_{\rm W} \geq 4.7$ and a minimum number of 6 intensity data points (IDPs).

Date and time	Lat. (°)	Lon. (°)	Depth (km)	$M_{\rm W}$	Epicentral intensity	Epicentral area	# IDPs
1295/09/03 –:–:–	46.78	9.54	Unknown	6.2	VIII	Churwalden, Alps	6
1356/10/18 21:–:–	47.47	7.60	Unknown	6.6	IX	Basel, Foreland	34
1584/03/11 11:30:00	46.33	6.97	10	5.9	VIII	Aigle, Alps	27
1601/09/18 01:–:–	46.92	8.36	10	5.9	VIII	Unterwalden, Alps	39
1650/09/21 03:–:–	47.55	7.53	Unknown	5.3	VII	Basel, Foreland	10
1685/03/08 19:–:–	46.28	7.63	Unknown	5.3	VII	Mittelwallis, Alps	13
1729/01/13 21:–:–	46.63	7.63	12	5.2	VI	Frutigen, Alps	23
1755/12/09 13:45:00	46.32	7.98	Unknown	5.7	VIII	Brig-Naters, Alps	86
1770/03/20 15:30:00	46.48	7.18	Unknown	5.2	VI	Chateau-d'Oex, Alps	8
1774/09/10 15:30:00	46.85	8.67	8	5.7	VII	Altdorf, Alps	56
1837/01/24 01:–:–	46.32	7.97	10	5.4	VII	Birgisch, Alps	38
1846/08/17 06:15:00	46.77	6.58	15	5.2	VI	Mathod-Yverdon-les-Bains, Foreland	15
1855/07/25 11:50:00	46.23	7.85	10	6.2	VIII	Stalden-Visp, Alps	101
1855/07/26 09:15:00	46.23	7.88	Unknown	5.5	VIII	Stalden-Visp, Alps	88
1880/07/04 08:20:00	46.22	7.80	Unknown	5.2	VII	Embd, Alps	33
1905/12/26 00:25:00	46.88	9.43	Unknown	4.7	VI	Tamins, Alps	96
1924/04/15 12:50:00	46.30	7.96	10	5.2	VII	Brig, Alps	65
1929/03/01 10:32:00	46.73	6.72	5	5	VII	Bioley-Magnoux, Foreland	117
1946/01/25 17:32:00	46.35	7.40	Unknown	5.8	VIII	Sierre, Alps	238
1946/05/30 03:41:00	46.30	7.42	Unknown	5.5	VII	Sierre, Alps	95
1954/05/19 09:35:00	46.28	7.31	10	5.3	VI	Mayens de My-Daillon, Alps	77
1964/03/14 02:39:00	46.867	8.317	5	5.3	VII	Sarnen, Alps	360
1991/11/20 01:54:18	46.731	9.527	6	4.7	VI	Vaz, Alps	373

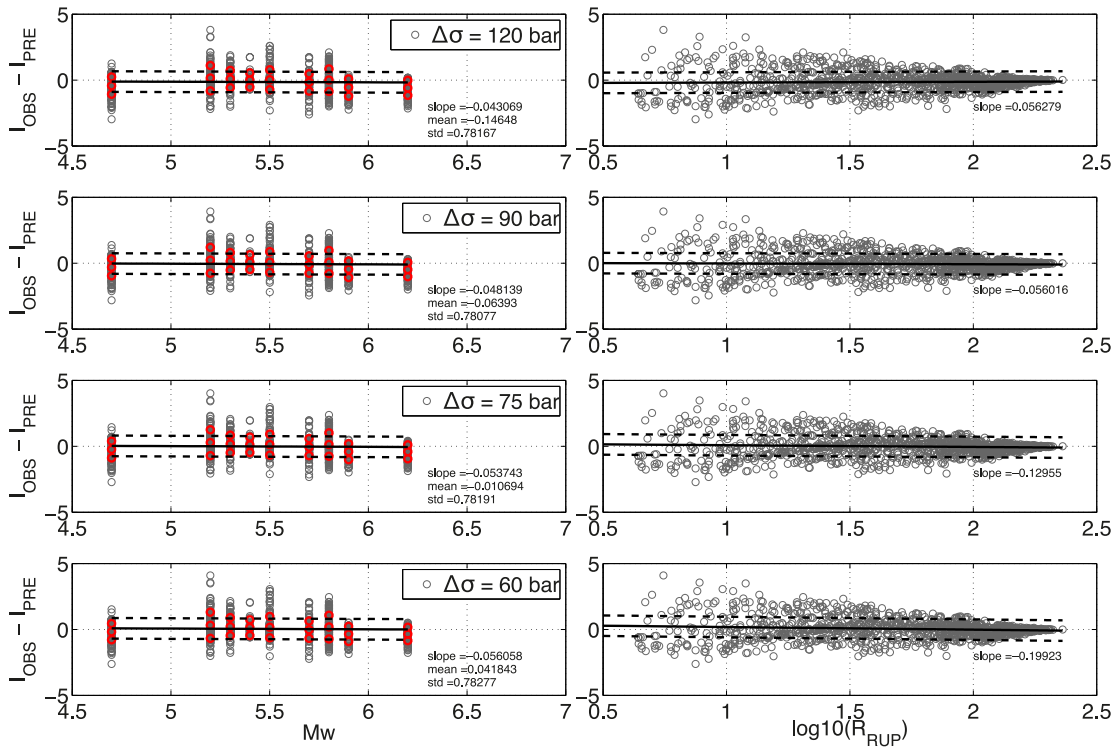

Figure 6. Alpine deep event (depth > 6 km) data set. Residuals (grey circles) are computed using the Swiss alpine stochastic model and plotted as a function of moment magnitude M_W and rupture distance R_{RUP}. Black lines: linear fitting of the residuals (with 1σ bounds). Red circles: mean $\pm 1\sigma$ of the residuals grouped by M_W values. The field 'slope' refers to the slope of the best-fitting straight line, while 'mean' and 'std' are the mean and standard error of the residuals, respectively.

and rupture geometries. This poses some practical issues as to the comparison with the parametrization of the Swiss stochastic model, where the distance from the ruptured fault R_{RUP} is used as predictor. To cope at least in part with this shortcoming, the epicentral distances of the historical catalogue were assumed equal to R_{JB} distances, and R_{JB} was subsequently converted into R_{RUP} based on an empirical equation calibrated on the synthetics data sets of EF13, where the depth of the simulated earthquakes is consistent with the depth distribution of the earthquakes in the instrumental catalogue of Switzerland (Fäh *et al.* 2011).

We compared the predicted IDPs (I_{PRE}) with the observed IDPs (I_{OBS}) by examining the magnitude and distance distributions of the residuals computed as:

$$residuals = I_{OBS} - I_{PRE}. \quad (9)$$

Note that the predicted and observed IDPs are treated here as continuous floating point values, that is the rounding strategy briefly discussed in Section 3 was not applied before computing the residuals. A distance-based weighting (w) scheme was applied to the residuals, similar to that used by Fäh *et al.* (2011) in developing the IPE based on the ECOS-09 catalogue, that is:

$$w = [(230 - R_{RUP})/230]^2, \quad (10)$$

where 230 km is the maximum epicentral distance in the data set. For the datapoints with predicted intensity lower than IV, only the ΔI_{rock} correction was retained and the site-specific intensity correction was removed from the computations. Eq. (10) was chosen after several preliminary investigations that included, amongst others, neglecting entirely the distance weighting or using a distance cut-off based on predicted macroseismic intensities smaller than IV. Neglecting the distance weighting of eq. (10) introduced a bias in the distribution of the residual with respect to both magnitude and distance, with clear underestimation of the IDPs in the near field and overestimation in the far field. Further, the overall spread of the residuals became larger. Introducing a distance cut-off based on predicted intensities lower than IV yielded strong trends in the distribution of the residuals as a function of magnitude.

The Swiss alpine and foreland IDPs were further segregated into a 'shallow' and a 'deep' subset, based on the focal depths of the events. This choice was driven by observing that, in both regions, merging the residuals computed for events with depth <6 km with the rest of the available data, resulted in strong trends in the distributions with distance and a clearly apparent overestimation of the IDPs in the near-field, irrespective of the $\Delta\sigma$ model that could better fit the available data. If unknown from the ECOS-09 catalogue, the focal depth was assumed, based on the depth distribution of the instrumental seismicity in Switzerland (Fäh *et al.* 2011).

For the Swiss alpine region, if we only consider the events with depth larger than 6 km, the most suitable models are those with maximum $\Delta\sigma$ ranging between 60 and 120 bar, as shown in Fig. 6. The LHS panels of Fig. 6 show the distribution of the residual as a function of M_W, while their variation with distance is given in the RHS panels. In each subplot, the solid line is the best-fitting straight line through the residuals, the dashed lines are its $\pm 1\sigma$ bounds.

For the Swiss foreland region and again for deep events (depth >6 km), we found that the most suitable models are characterized by maximum $\Delta\sigma$ values between 50 and 90 bar, as shown in Fig. 7.

In both regions, fitting the historical IDPs of events with focal depth <6 km required using lower $\Delta\sigma$ values, typically ranging between 10 and 30 bar, as shown in Fig. 8 for the events that occurred in the Swiss Alps (only one event is available in the foreland region).

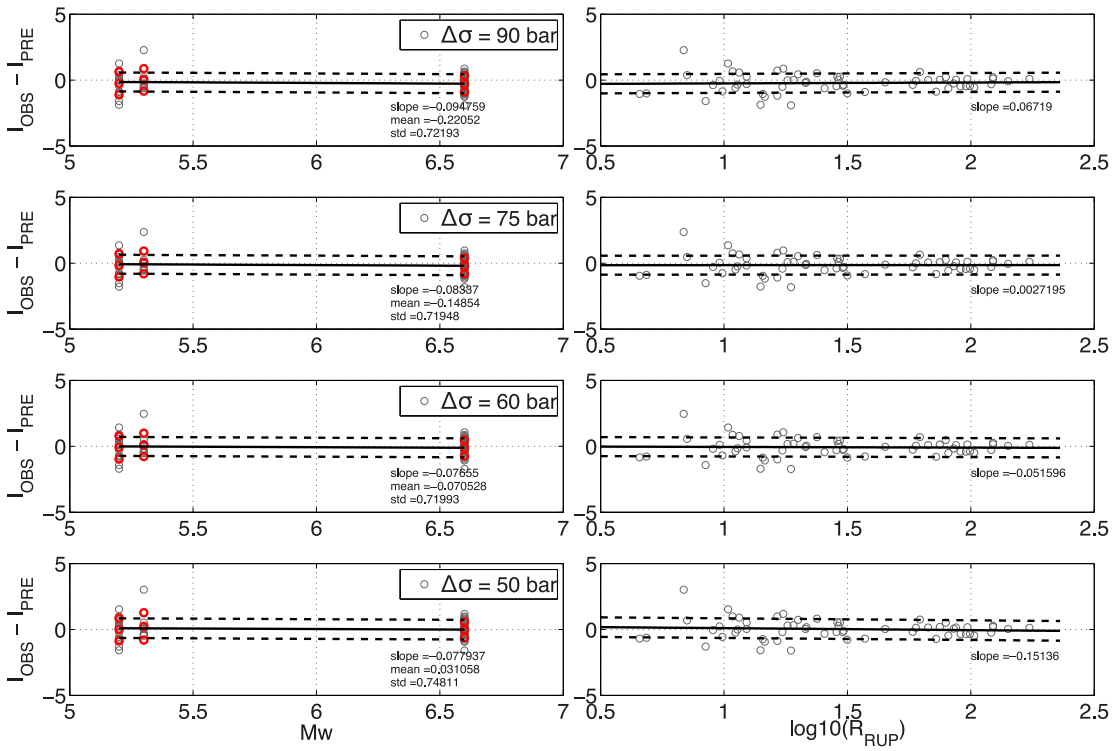

Figure 7. As Fig. 6, but for the deep events (depth > 6 km) that occurred in the Swiss Foreland.

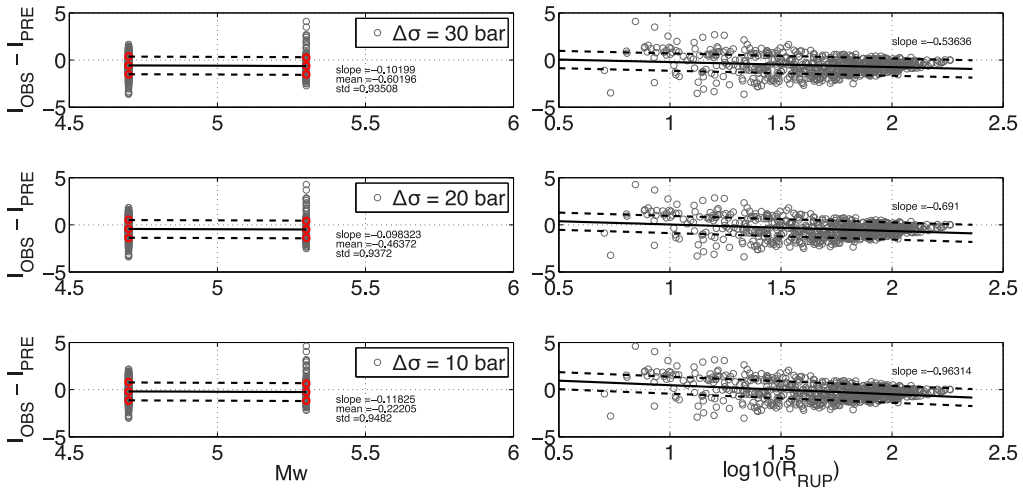

Figure 8. As Figs 6 and 7, but for the shallow events (depth < 6 km) that occurred in the Swiss alpine region.

This behaviour, that is the increase of the stress-drop with depth, is partially confirmed by observations based on recent instrumental seismicity in Switzerland, where average stress-drops greater than around 30 bars were only found at depth (Goertz-Allmann & Edwards 2014). Interpretation of earthquake stress-drop is, however, rather uncertain, with results depending strongly on method and assumptions. For instance, the apparent increase of stress drop with depth shown by Goertz-Allmann & Edwards (2014), disappeared if assuming (and accounting for) a depth dependent attenuation structure. A further limitation of this interpretation is that stress-drop must increase with moment magnitude to satisfy both Swiss instrumental and macroseismic observations. This means that as magnitude increases, our uncertainty regarding the depth dependence of stress-drop increases, since no large magnitude events have been recorded instrumentally in Switzerland. The largest moment magnitudes in the Swiss instrumental catalogue do not exceed 4.4.

6 SHAKING SCENARIOS FOR HISTORICAL AND INSTRUMENTAL EVENTS

We present intensity shaking scenarios obtained using the previous *SEDShakeMap32* and new *SEDShakeMap35* for historical and recent instrumental events in Switzerland. The chosen historical scenarios (see Table 1) refer to possible repetitions of (1) the M_W 6.6 (Fäh *et al.* 2011) 1356 Basel event (Swiss foreland region) and (2) the M_W 6.2 (Fäh *et al.* 2011) 1855 Visp-Stalden earthquake (Swiss alpine region). In addition, we present intensity-based shaking

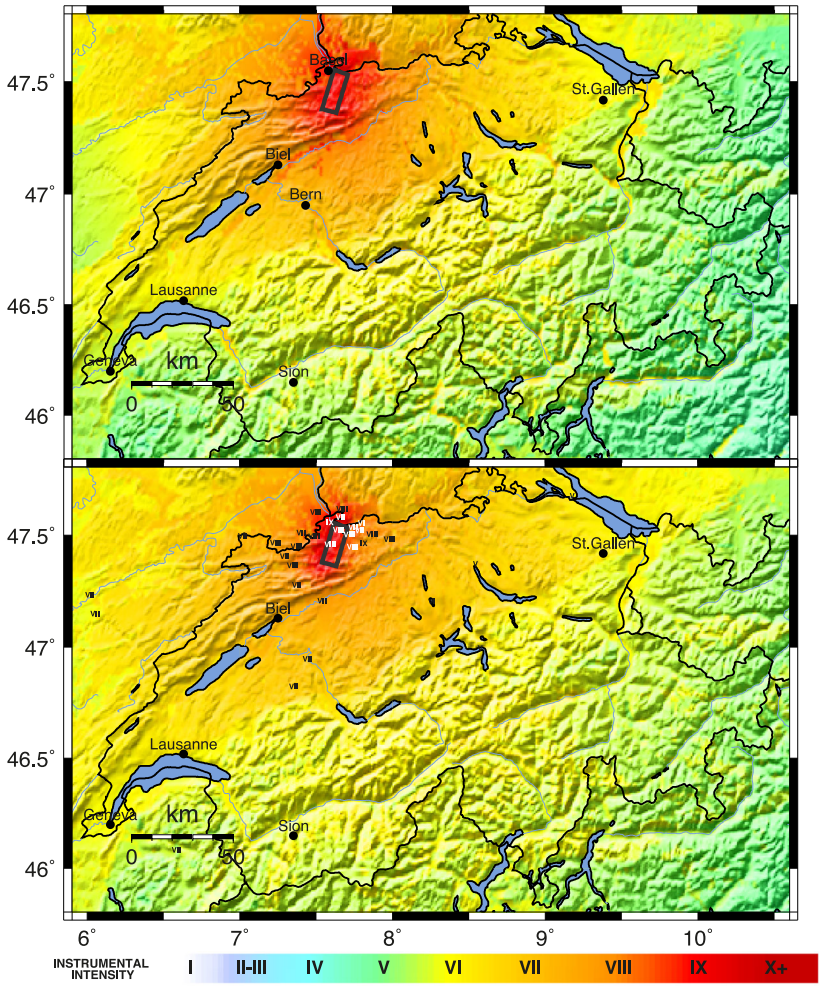

Figure 9. Intensity shaking scenario based on the M_W 6.6 1356 Basel event. Top panel: SEDShakeMap32 computations, using CH08, KF06 and the site amplification estimates of Cua *et al.* (2007). Bottom panel: SEDShakeMap35 scenario, based on EF13, FM10 and the amplification factors described in Section 4. The bottom panel also includes intensity records available in the ECOS-09 catalogue.

scenarios for the two recent Swiss events introduced in Section 2. For the instrumental events we computed both shaking scenarios and *ShakeMaps*, the latter also being constrained by observed seismic station records. The M_W values to be used in EF13 for the instrumental earthquake scenarios were computed from M_L using the Swiss specific conversion equations of Goertz-Allmann *et al.* (2011). Based on the residual analyses presented in the previous section, a simplified logic-tree approach was adopted for the *SEDShakeMap35* scenarios and *ShakeMaps*. For events occurring in the Swiss foreland region, the weighted average of EF13(50 bar), EF13(60 bar), EF13(75 bar) and EF13(90 bar) was used with weights equal to 0.35, 0.35, 0.2 and 0.1, respectively. For earthquakes located in the Swiss alpine region, the chosen $\Delta\sigma$ values were 60, 75, 90 and 120 bar, with weights again equal to 0.35, 0.35, 0.2 and 0.1, respectively.

The M_W 6.6 earthquake that occurred in Basel in 1356 is one of the most damaging events in the seismic catalogue of intraplate Europe. Due to its significance in regional seismic hazard studies in central Europe, this earthquake has been the subject of several multidisciplinary research projects incorporating investigation techniques from history, seismology, archaeology, palaeoseismology and engineering. Macroseimic intensity reached degree IX in the city of Basel, and intensities up to degree VIII were found within a radius of 30 km (Fäh *et al.* 2009; Schwarz-Zanetti & Fäh 2011). The epicentre was most likely located some 10 km south of Basel, along the linear Basel–Reinach fault scarp, an active normal fault striking NNE–SSW and dipping ∼65° to the East. Based on morphology, the along-strike extension of the fault could have reached approximately 20 km across the Jura Mountains and the Rhine valley (Ferry *et al.* 2005). A simplified rectangular representation of the causative fault of the 1356 event is depicted in Fig. 9 (grey rectangles in top and bottom panels). The along-strike length of the fault $L \sim 20$ km and its down-dip extension $W \sim 17.5$ km were computed based on Wells & Coppersmith (1994). The top panel of Fig. 9 shows the *SEDShakeMap32* scenario (using CH08, KF06 and the site amplification estimates of Cua *et al.* 2007), while depicted in the bottom panel is the *SEDShakeMap35* scenario, based on EF13, FM10 and the amplification factors described in Section 4. In the bottom panel, the intensity data records available in the ECOS-09 catalogue are also shown for comparison with the earthquake scenario. Consistent with the historical observations, macroseismic intensity reaches (and actually exceeds at a few gridpoints) degree IX in the near-source region and in the city of Basel. The area affected by intensity IX is larger in the top panel, where it extends for ∼10 km outside the surface projection of the ruptured fault. This is mainly due to the use of the Joyner–Boore distance metric (R_{JB}) in CH08. In the bottom panel, where the rupture distance R_{RUP} of EF13 is used, the area characterized by intensity IX is located around the

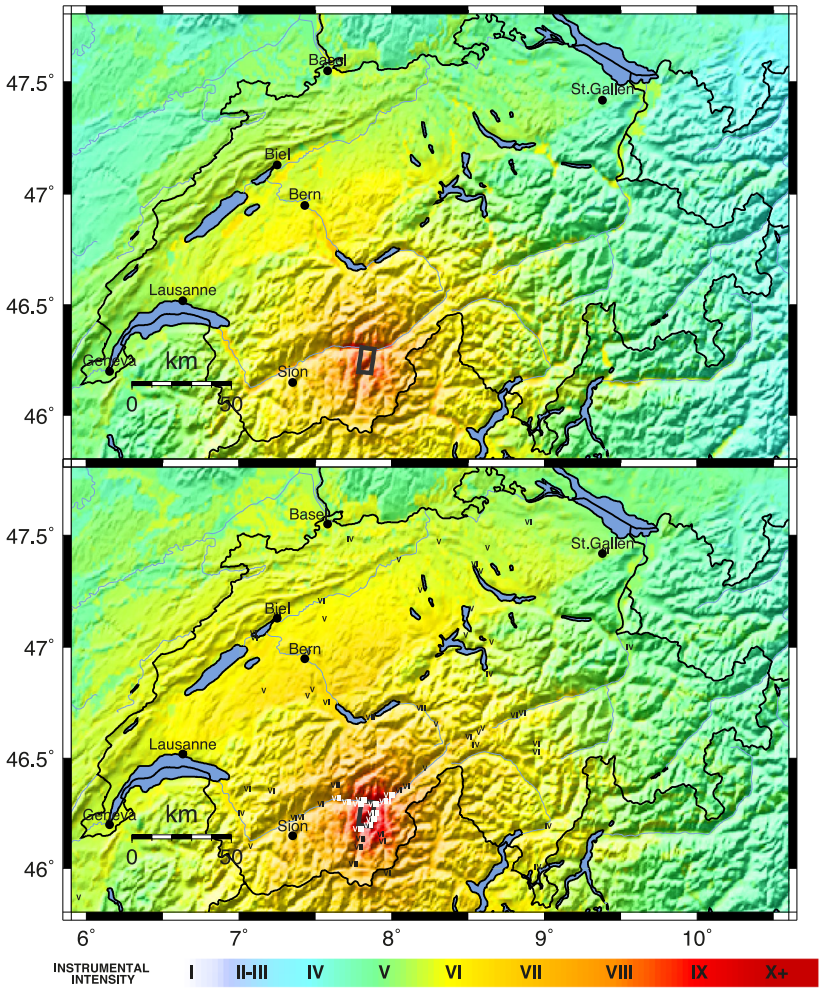

Figure 10. Same as Fig. 9, for the M_W 6.2 1855 Visp-Stalden event.

surface expression of the fault to the west. While both scenarios are in good agreement with the historical macroseismic observations (see also Fäh *et al.* 2009, their figs 10 and 11), it is apparent from of Fig. 9 that predicted intensities in *SEDShakeMap32* are larger than *SEDShakeMap35* in the Swiss foreland region, and lower in the eastern Alps.

On 1855 July 25, the alpine area of central Valais was hit by a M_W 6.2 (Fäh *et al.* 2011) earthquake, the largest event to have occurred in Switzerland in the last 300 yr. The intensity shaking reached degree VIII in the epicentral region and damage was observed in a wide area around the town of Visp. The main shock was followed by dozens of damaging aftershocks in the subsequent months and years, all located near the towns of Stalden and Visp (Fritsche *et al.* 2006; Gisler & Fäh 2011). The damage pattern associated to the main shock and the geographical distribution of the aftershocks are consistent with a rupture occurring on a normal fault, close to the surface, striking approximately NS along the Valley of Visp and dipping ∼60° to the west (Fritsche *et al.* 2006). A simplified rectangular representation of the causative fault of the 1855 Visp-Stalden event is shown in Fig. 10 (grey rectangles in top and bottom panels). Based on Wells & Coppersmith (1994), we assumed $L \sim 12.5$ km and $W \sim 13.5$. Similar to Fig. 9, the top panel of Fig. 10 shows the *SEDShakeMap32*, while the *SEDShakeMap35* is depicted in the bottom panel, along with the IDPs available in ECOS-09. For this scenario, both *SEDShakeMap32* and *SEDShakeMap35* tend to exceed intensity VIII by approximately 0.5 intensity units, and therefore overestimate the intensity levels based on the historical reports in the near-source region. The overestimation is more pronounced for *SEDShakeMap35*, close to the surface expression of the ruptured fault, to the east. The predicted shaking levels are higher for *SEDShakeMap35* in the Swiss foreland, while only minor differences between the two implementations can be appreciated throughout the Swiss Alps, in the far-field region. Note how the *SEDShakeMap35* near-source predictions are only slightly lower than those shown in the bottom panel of Fig. 9. This is consistent with the generally higher amplitudes predicted (for a given magnitude) by EF13 in the alpine region with respect to the Swiss Foreland.

The M_L 4.2 2012 Zug earthquake (Diehl *et al.* 2013) was the strongest earthquake to occur within Swiss borders since 1999. The event was located at ∼32 km depth, 2 km above the Moho at this location according to the crustal model of Wagner *et al.* (2012). Although a well-constrained fault-plane solution was derived by Diehl *et al.* (2013), the size of the event is small enough to justify the computation of shaking scenarios based on a point-source representation, as shown in Fig. 11. The left-hand panels of Fig. 11 show intensity shaking scenarios from *SEDShakeMap32* (top panel) and *SEDShakeMap35* (bottom panel) based only on GMPEs, GMICEs and regional site effect estimates. In the right-hand panels, consistent with the classical *ShakeMap* approach, the peak ground

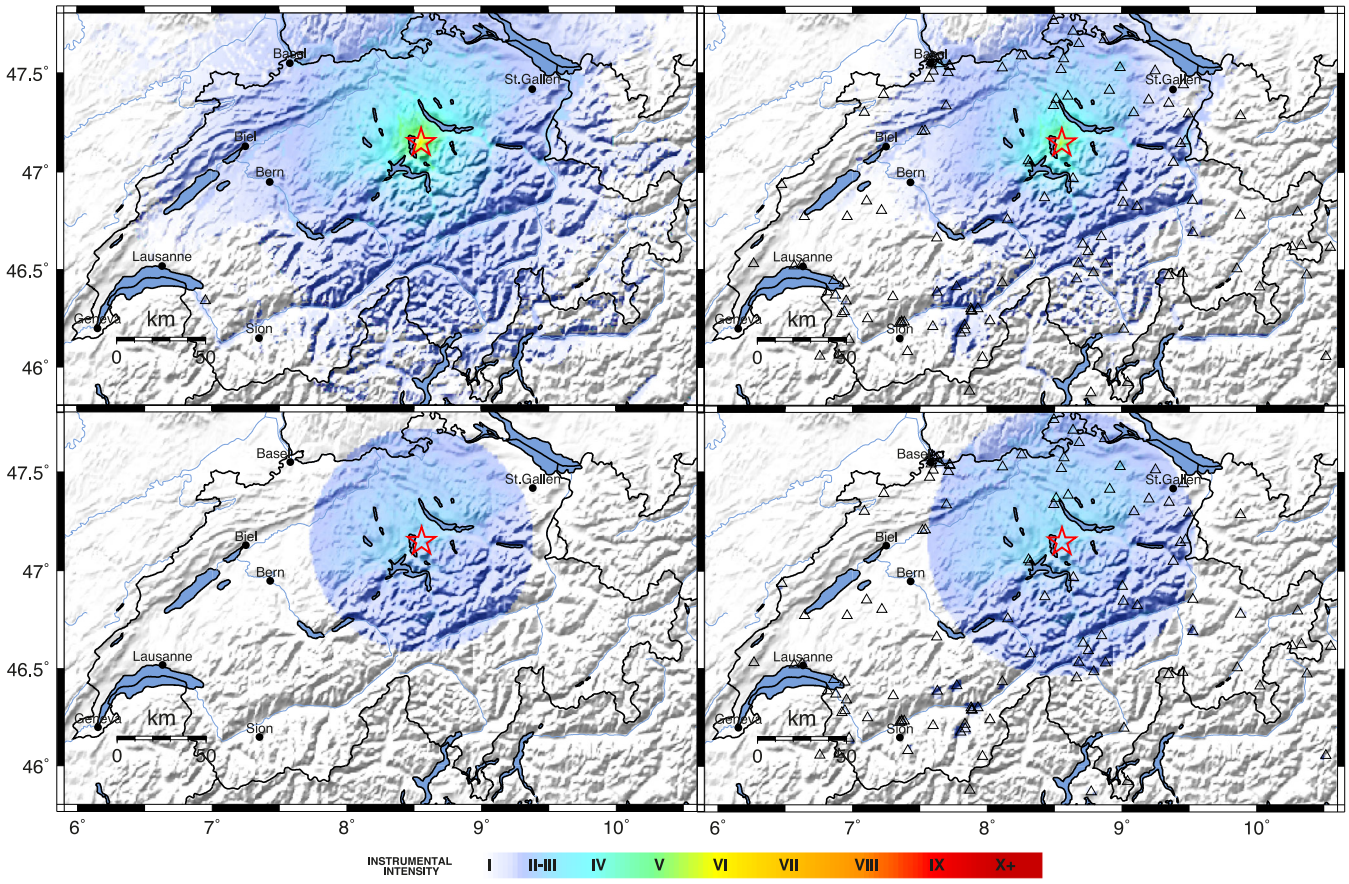

Figure 11. Intensity shaking scenarios (left-hand panels) and ShakeMaps (right-hand panels) for the M_L 4.2 event occurred near Zug on 2012 February 11, computed as explained in the text. Top panels: SEDShakeMap32. Bottom panels: SEDShakeMap35, with radius of influence of seismic stations equal to 2 km. In all panels, the red star is the epicentre. The triangles in the right-hand side panels are the seismic stations that recorded the event.

motion information at the recording sites is additionally used to constrain the spatial distribution of the shaking levels. The *SEDShakeMap32* scenario (top left-hand panel) shows intensity levels as high as degree V–VI (from strong shaking to slightly damaging shaking) and suggests that the earthquake could have been felt across a very large area encompassing the Swiss foreland region and the central-eastern Swiss Alps. After inclusion of the information available at the recording stations (top right-hand panel), the area affected by predicted intensities larger than or equal to degree II (scarcely felt) is reduced to eastern Switzerland and the central Valais. The epicentral intensity is also reduced by approximately one degree. The epicentral intensity predicted by *SEDShakeMap35* (left bottom-hand panel) is considerably lower than that of *SEDShakemap32*, ranging between degree III and IV. Intensities larger than or equal to degree II are predicted within approximately 65 km of the earthquake epicentre. Once the station recordings are included in the shaking scenario (bottom right-hand panel), intensities in the epicentral area and in the eastern Swiss foreland approach degree IV, and the radius of the region where the earthquake was potentially felt increases to approximately 75 km. The *SEDShakeMap35* scenario is consistent with the macroseismic reports collected by the SED: the epicentral intensity of the main shock was IV, with a relatively 'flat' intensity field typical of deep events. The main shock was widely felt in the eastern and central Alpine foreland, spreading to the eastern extensions of the Jura mountain range, to the Basel area and to Lake Constance. Significantly fewer reports were received from the southern and western parts of Switzerland and the Alpine area as a whole (Diehl *et al.* 2013). The differences observed between *SEDShakeMap32* and *SEDShakeMap35* are mainly due to the different distance metrics used in the GMPEs. Based on R_{JB} (roughly equal to the epicentral distance R_E for events of this size) and a constant fictitious depth of 3 km, CH08 is insensitive to the actual depth of the earthquake. Conversely, the depth of the earthquake focus is implicitly taken into account by EF13 by using R_{RUP}, basically equal to the focal depth R for low energy events.

On 2013 December 12, an earthquake with a local magnitude M_L of 4.1 occurred in the Rhine valley, close to the village of Balzers in southern Lichtenstein. Focal depth is estimated to be 7 ± 2 km. As many people were at rest (if not asleep—the origin time was 00:50 am UTC), the event was widely felt in the Alpine Rhine valley from Chur towards Lake Constance, across the entire Liechtenstein and in adjacent areas of Switzerland and Austria. While the manual analysis of the macroseismic reports received by the SED is still ongoing, automatically generated felt reports suggested a preliminary intensity of ~IV degree in the epicentral area. Similar to the approach followed for the Zug event, the *SEDShakeMap32* and *SEDShakeMap35* scenarios of the Balzers event are shown in Fig. 12. As expected based on the magnitude of the earthquake, the top left-hand panel of Fig. 12, *SEDShakeMap32* unconstrained by data, shows epicentral intensity levels (V–VI) and the spatial extent of intensity larger than or equal to II is similar to the Zug event. The epicentral intensity is reduced by more than one degree and the felt radius is dramatically reduced after inclusion

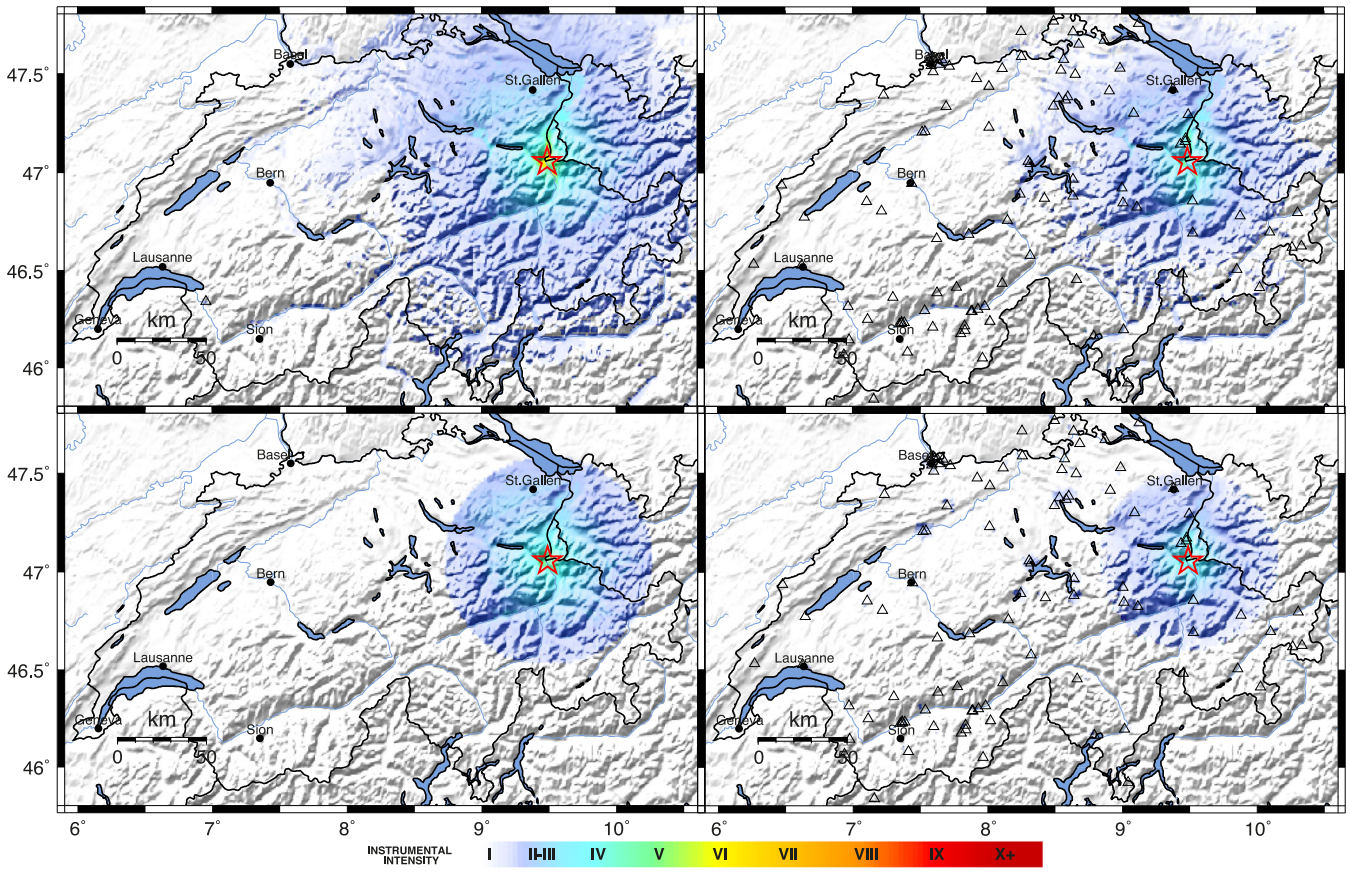

Figure 12. Same as Fig. 11, for the M_L 4.1 event occurred in Balzers on 2013 December 12.

of the information available at the recording sites (top right-hand panel). *SEDShakeMap35* predicts in this case an epicentral intensity approaching degree V and a felt radius of ∼60 km. The estimated epicentral intensity decreases to ∼IV after the inclusion of the available seismic recordings (bottom right-hand panel). The felt radius is then reduced to ∼50 km, although intensity levels approaching degree II are predicted at a few seismic stations located in the central Swiss foreland and alpine region. Overall, given the relatively shallow depth of the earthquake at hand, a fair agreement is observed between *SEDShakeMap32* and *SEDShakeMap35*, the latter being more consistent with the preliminary automatic computation of the macroseimic intensity field.

For both the Zug and the Balzers event, the shape (circular) of the region characterized by intensities larger than II of *SEDShakeMap35* is remarkably different from *SEDShakeMap32* and is most likely governed by the fundamental revision of the previous *ShakeMap* methodology carried out by Worden *et al.* (2010).

7 DISCUSSION AND CONCLUSIONS

In this study, we presented a comprehensive revision of the scientific and technical background of the Swiss customization of *ShakeMap*, in use since 2007 at the SED. This work is spurred by the recent network enhancements and scientific developments in the domain of engineering seismology in Switzerland.

The new *ShakeMaps* rely on an *ad-hoc* developed set of GMPEs based on the stochastic model of Edwards & Fäh (2013), which was specifically developed for earthquake ground-motion predictions over a broad magnitude and distance range in Switzerland. Using synthetics overcomes the difficulties posed by: (i) the paucity of strong-motion data recordings in Switzerland; (ii) the regional dependence of shear-wave energy attenuation and focal depth distribution in the Swiss Alps and foreland and (iii) the depth dependence of stress parameters suggested by macroseismic and instrumental observations. In order to be able to optimize flexibility of the predictive tool, the synthetics-based GMPEs encompass a wide range of possible stress-drop values, from 10 to 120 bar, although retaining the same functional form. The GMPEs use the finite-fault distance metric R_{RUP} as predictor (basically equal to the focal distance for low-energy events), but they do not include style-of-faulting (Bommer *et al.* 2003), directivity (Somerville *et al.* 1997) and hanging-wall (e.g. Abrahamson & Somerville 1996) terms, which would be of little or no use in near-real-time applications. Nevertheless, we are aware that the inclusion of these corrective terms in the GMPEs may be critical to adequately assess the level of near-source shaking for large damaging events, similar to, for example the 1356 Basel or 1855 Visp-Stalden earthquakes, discussed in the paper. For such planning-scenario purposes, the aforementioned GMPE modifiers can be adapted from those available in the international literature. Indeed, style-of-faulting terms are nowadays routinely included into state-of-the-art empirical GMPEs (e.g. Douglas *et al.* 2014; Gregor *et al.* 2014) and the hanging-wall effect (that might be implicitly taken into account by modelling ground-motion attenuation as a function of R_{JB}) is typically parametrized as a function of R_X, the horizontal distance from the top edge of the rupture, measured perpendicular to the fault strike (e.g. Chiou & Youngs 2014). As to the inclusion of directivity effects in GMPEs, use can

be made, for example, of the recent findings of the NGA-West2 Directivity Working Group (Spudich *et al.* 2014).

In the new Swiss *ShakeMap*, the expected amplification of ground-shaking at regional scale is derived from amplification factors of macroseismic intensity for different soil classes, based on the recently revised earthquake catalogue of Switzerland (ECOS-09; Fäh *et al.* 2011). One potential drawback of the new implementation is that, although plastic soil behaviour is expected to be implicitly taken into account in the calibration data set, the amplification factors are applied as constant modifiers, irrespective of magnitude and distance. Although this design choice can be verified and better refined in the future, we believe it is a reasonable and conservative assumption for typical *ShakeMap* applications. At a seismic station level, following Edwards *et al.* (2013), the soil class amplification factors are substituted by the actual recorded amplification with respect to the Swiss reference rock model of Poggi *et al.* (2011). These latter amplification values may vary with time, once new relevant earthquakes are recorded at the monitoring sites.

The new implementation described in this article converts ground-motion levels into macroseismic intensity based on the GMICE of Faenza & Michelini (2010) to take full advantage of their enhanced strong-motion and intensity observation database, well constrained for intensities larger than VII.

The combination of all these new features within the *ShakeMap* software framework (version 3.5) freely distributed by the United States Geological Survey (USGS) constitutes the basis of the next-generation Swiss *ShakeMap*. Shaking scenarios based on the new implementation showed a satisfactory agreement with the macroseimic fields of both large historical events and recent well-recorded earthquakes of moderate magnitude. The new implementation is now fully consistent with the state-of-the-art in engineering seismology in Switzerland.

ACKNOWLEDGEMENTS

The open-source software module scwfparam used for rapid parametrization of waveforms data in SeisComP3 has been developed by the Swiss Seismological Service and gempa GmbH within the framework of the EC-funded project NERA, and received support from Geoscience Australia and GNS Science, New Zealand. We are grateful to the ShakeMap working group (in particular Bruce Worden and David Wald) at the USGS for maintaining the core ShakeMap modules and making them freely available to the community. We are thankful to David Wald for his encouragement of the development and publication of this work in the international literature, and to two anonymous colleagues for reviewing the original manuscript and for providing useful suggestions for improvements. The waveform data and station metadata of the Swiss national monitoring networks are openly available through the ArcLink server and web interface accessible at http://arclink.ethz.ch (last accessed 3 November 2014). This work was partly funded by the Swiss Nuclear Safety Inspectorate (ENSI).

REFERENCES

Abrahamson, N.A. & Somerville, P.G., 1996. Effects of the hanging wall and footwall on ground motions recorded during the Northridge earthquake, *Bull. seism. Soc. Am.,* **86**(B1), S93–S99.

Akkar, S., Sandıkkaya, M.A. & Bommer, J.J., 2014. Empirical ground-motion models for point- and extended-source crustal earthquake scenarios in Europe and the Middle East, *Bull. Earthq. Eng.,* **12**(1), 359–387.

Atkinson, G.M., Assatourians, K., Boore, D.M., Campbell, K. & Motazedian, D., 2009. A guide to differences between stochastic point-source and stochastic finite-fault simulations, *Bull. seism. Soc. Am.,* **99**(6), 3192–3201.

Bay, F.D., Malagnini, L. & Giardini, D., 2003. Spectral shear-wave ground-motion scaling in Switzerland, *Bull. seism. Soc. Am,* **93,** 414–429.

Bommer, J.J., Douglas, J. & Strasser, F.O., 2003. Style-of-faulting in ground-motion prediction equations, *Bull. Earthq. Eng.,* **1**(2), 171–203.

Boore, D.M., 2009. Comparing stochastic point-source and finite-source ground-motion simulations: SMSIM and EXSIM, *Bull. seism. Soc. Am.,* **99**(6), 3202–3216.

Boore, D.M., Stewart, J.P., Seyhan, E. & Atkinson, G.M., 2014. NGA-west 2 equations for predicting PGA, PGV, and 5%-damped PSA for shallow crustal earthquakes, *Earthq. Spectra,* **30,** 1057–1085.

Burger, R., Somerville, P., Barker, J., Herrmann, R. & Helmberger, D., 1987. The effect of crustal structure on strong ground motion attenuation relations in eastern North America, *Bull. seism. Soc. Am.,* **77,** 420–439.

Cauzzi, C. & Clinton, J., 2013. A high- and low-noise model for high-quality strong-motion accelerometer stations, *Earthq. Spectra,* **29**(1), 85–102.

Cauzzi, C. & Faccioli, E., 2008. Broadband (0.05 to 20 s) prediction of displacement response spectra based on worldwide digital records, *J. Seismol.,* **12**(4), 453–475.

Cauzzi, C., Clinton, J., Becker, J. & Kästli, P., 2013. Scwfparam: a tool for rapid parameterisation of ground motions and input to ShakeMap in SeisComP3, *Seismol. Res. Lett.,* **84**(2), 356, doi:10.1785/0220130011.

Cauzzi, C., Faccioli, E., Vanini, M. & Bianchini, A., 2014. Updated predictive equations for broadband (0.01 to 10 s) horizontal response spectra and peak ground motions, based on a global dataset of digital acceleration records, *Bull. Earthq. Eng.*, doi:10.1007/s10518-014-9685-y.

Chiou, B., Darrag, R., Gregor, N. & Silva, W., 2008. NGA project strong-motion database, *Earthq. Spectra,* **24**(1), 23–44.

Chiou, B.S.-J. & Youngs, R.R., 2014. Update of the Chiou and Youngs NGA model for the average horizontal component of peak ground motion and response spectra, *Earthq. Spectra,* **30**(3), 1117–1153.

Clinton, J. *et al.*, 2011. The current state of strong motion monitoring in Switzerland, in *Earthquake Data in Engineering Seismology*, pp. 219–233, eds Akkar, S., Gülkan, P. & van Eck, T., Springer.

Cua, G. & Heaton, T., 2008. New ground motion prediction equations spanning weak and strong motion levels, in *Proceedings of the American Geophysical Union Fall Meeting*, San Francisco, CA, Paper no. S51A-0230.

Cua, G., Kaesti, P., Fäh, D., Wiemer, S., Clinton, J. & Giardini, D., 2007. Deriving Vs30 maps for Switzerland from macroseismic intenisty data, in *Proceedings of the American Geophysical Union Fall Meeting*, San Francisco, CA, Paper no. S51A-0216.

Deichmann, N., 2010. *Summary of Earthquake Focal Mechanisms in Northern Switzerland*, Report to PEGASOS Refinement Project, 2010/11/01.

Delavaud, E. *et al.*, 2012. Toward a ground-motion logic tree for probabilistic seismic hazard assessment in Europe, *J. Seismol.,* **16**(3), 451–473.

Diehl, T. *et al.*, 2013. Earthquakes in Switzerland and surrounding regions during 2012, *Swiss J. Geosci.,* **106,** 543–558.

Diehl, T. *et al.*, 2014. Earthquakes in Switzerland and surrounding regions during 2013, *Swiss J. Geosci.*, doi:10.1007/s00015-014-0171-y.

Douglas, J. *et al.*, 2014. Comparisons among the five ground-motion models developed using RESORCE for the prediction of response spectral accelerations due to earthquakes in Europe and the Middle East, *Bull. Earthq. Eng.,* **12**(1), 341–358.

Edwards, B. & Fäh, D., 2013. A stochastic ground-motion model for Switzerland, *Bull. seism. Soc. Am.,* **103**(1), 78–98.

Edwards, B., Fäh, D. & Giardini, D., 2011. Attenuation of seismic shear wave energy in Switzerland, *Geophys. J. Int.,* **185**(2), 967–984.

Edwards, B., Michel, C., Poggi, V. & Fäh, D., 2013. Determination of site amplification from regional seismicity: application to the Swiss national seismic networks, *Seismol. Res. Lett.,* **84**(4), 611–621.

Faccioli, E., Villani, M., Vanini, M. & Cauzzi, C., 2010. Mapping seismic hazard for the needs of displacement-based design: the case of Italy, in *Advances in Performance-Based Earthquake Engineering*, pp. 3–14, ed. Fardis, M.N., Springer Netherlands, Dordrecht.

Faenza, L. & Michelini, A., 2010. Regression analysis of MCS intensity

and ground motion parameters in Italy and its application in ShakeMap, *Geophys. J. Int.,* **180**(3), 1138–1152.
Faenza, L. & Michelini, A., 2011. Regression analysis of MCS intensity and ground motion spectral accelerations (SAs) in Italy, *Geophys. J. Int.,* **186**(3), 1415–1430.
Fäh, D., 1985. Seismische Mikrozonierung der Schweiz, *Diploma thesis*, Institute of Geophysics, Swiss Federal Institute of Technology ETH, Zürich.
Fäh, D. *et al.*, 2003. Earthquake Catalogue of Switzerland (ECOS) and the related macroseismic database, *Eclogae geol. Helv. – Swiss J. Geosci.,* **96,** 219–236.
Fäh, D. *et al.*, 2009. The 1356 Basel earthquake: an interdisciplinary revision, *Geophys. J. Int.,* **178**(1), 351–374.
Fäh, D. *et al.*, 2011, ECOS-09 Earthquake Catalogue of Switzerland, Release 2011 Report and Database, Swiss Seismological Service ETH Zurich, Report SED/RISK/R/001/20110417.
Ferry, M., Meghraoui, M., Delouis, B. & Giardini, D., 2005. Evidence for Holocene palaeoseismicity along the Basel-Reinach active normal fault (Switzerland): a seismic source for the 1356 earthquake in the Upper Rhine graben, *Geophys. J. Int.,* **160**(2), 554–572.
Fritsche, S., Fäh, D., Gisler, M. & Giardini, D., 2006. Reconstructing the damage field of the 1855 earthquake in Switzerland: historical investigations on a well-documented event, *Geophys. J. Int.,* **166**(2), 719–731.
Gisler, M. & Fäh, D., 2011. Grundlagen des Makroseismischen Erdbebenkatalogs der Schweiz. 1681–1878, in *Herausgegeben vom Schweizerischen Erdbebendienst,* Zürich. vdf, 2011, pp 185. Download open access: ISBN 978-3-7281-3407-3, doi:10.3218/3407-3.
Goertz-Allmann, B.P., Edwards, B., Bethmann, F., Deichmann, N., Clinton, J., Fah, D. & Giardini, D., 2011. A new empirical magnitude scaling relation for Switzerland, *Bull. seism. Soc. Am.,* **101**(6), 3088–3095.
Goertz-Allmann, B.P. & Edwards, B., 2014. Constraints on crustal attenuation and three-dimensional spatial distribution of stress drop in Switzerland, *Geophys. J. Int.,* **196,** 493–509.
Gregor, N. *et al.*, 2014. Comparison of NGA-West2 GMPEs, *Earthq. Spectra,* **30,** 1179–1197.
Grünthal, G., 1998. European macroseismic scale 1998 (EMS-98), Cahiers du Centre Européen de Géodynamique et de Séismologie, 15.
Grünthal, G. & Levret, A., 2001. L'Echelle Macrosismique Européenne. European macroseismic scale 1998 (EMS-98), Cahiers du Centre Européen de Géodynamique et de Séismologie, 19.
Hanka, W., Saul, J., Weber, B., Becker, J. & Harjadi, P., 2010. Real-time earthquake monitoring for tsunami warning in the Indian Ocean and beyond, *Nat. Hazards Earth Syst. Sci.,* **10**(12), 2611–2622.
Joyner, W.B. & Boore, D.M., 1981. Peak horizontal acceleration and velocity from strong-motion records including records from the 1979 imperial valley, California, earthquake, *Bull. seism. Soc. Am.,* **71**(6), 2011–2038.
Kästli, P. & Fäh, D., 2006. Rapid estimation of macroseismic effects and shake maps combining macroseismic and instrumental data, in *Proceedings of the First European Conference on Earthquake Engineering and Seismology (ECEES)*, Geneva, Switzerland, Paper no. 1535.
Michel, C., Edwards, B., Poggi, V., Burjánek, J., Roten, D., Cauzzi, C. & Fäh, D., 2014. Assessment of site effects in Alpine regions through systematic site characterization of seismic stations, *Bull. seism. Soc. Am.* **104**(6), doi:10.1785/0120140097.
Musson, R.M.W., Grünthal, G. & Stucchi, M., 2009. The comparison of macroseismic intensity scales, *J. Seismol.,* **14**(2), 413–428.
Pacor, F. *et al.*, 2011. Overview of the Italian strong motion database ITACA 1.0, *Bull. Earthq. Eng.,* **9**(6), 1723–1739.
Poggi, V., Edwards, B. & Fäh, D., 2011. Derivation of a reference shear-wave velocity model from empirical site amplification, *Bull. seism. Soc. Am.,* **101**(1), 258–274.
Schwarz-Zanetti, G. & Fäh, D., 2011. Grundlagen des Makroseismischen Erdbebenkatalogs der Schweiz 1000–1680, Herausgegeben vom Schweizerischen Erdbebendienst, Zürich, doi:10.3218/3406-6.
Somerville, P.G., Smith, N.F., Graves, R.W. & Abrahamson, N.A., 1997. Modification of empirical strong ground motion attenuation relations to include the amplitude and duration effects of rupture directivity, *Seismol. Res. Lett.,* **68**(1), 222–991.
Spudich, P., Rowshandel, B., Shahi, S., Baker, J.W. & Chiou, B.S.-J., 2014. Comparison of NGA-West2 directivity models, *Earthq. Spectra,* **30**(3), 1199–1221.
Wagner, M., Kissling, E. & Husen, S., 2012. Combining controlled-source seismology and local earthquake tomography to derive a 3-D crustal model of the western Alpine region, *Geophys. J. Int.,* **191**(2), 789–802.
Wald, D.J., Quitoriano, V., Heaton, T.H., Kanamori, H., Scrivner, C.W. & Worden, C.B., 1999. TriNet "ShakeMaps": rapid generation of peak ground motion and intensity maps for earthquakes in Southern California, *Earthq. Spectra,* **15**(3), 537–555.
Wald, D.J., Worden, B.C., Quitoriano, V. & Pankow, K.L., 2005. ShakeMap manual: users guide, Technical manual, and software guide, USGS Techniques and Methods, 12-A1.
Wells, D.L. & Coppersmith, K.J., 1994. New empirical relationships among magnitude, rupture length, rupture width, rupture area, and surface displacement, *Bull. seism. Soc. Am.,* **84**(4), 974–1002.
Worden, C.B., Wald, D.J., Allen, T.I., Lin, K., Garcia, D. & Cua, G., 2010. A revised ground-motion and intensity interpolation scheme for ShakeMap, *Bull. seism. Soc. Am.,* **100**(6), 3083–3096.

APPENDIX

We present in this appendix a comparison of EF13 with popular empirical predictive equations in use in Switzerland and in Europe, namely: the previously adopted model Cua & Heaton (2008) CH08, the recently published Pan-European predictive equations of Akkar *et al.* (2014), ASB14, and the global broad-band prediction model of Cauzzi & Faccioli (2008), CF08. This appendix is not aimed at testing the Swiss stochastic prediction model against empirical GMPEs, as a rigorous testing would suffer from the assumptions necessary to accommodate the use of different calibration data sets, reference $V_{S,30}$ and distance metrics. Rather—and to some extent similar to Edwards & Fäh (2013, their figs 16 and 17)—we provide the reader with additional information useful to appreciate the behaviour of EF13 with respect to empirical prediction tools he/ she might be more familiar with.

Shown in Fig. A1 are the comparisons amongst the predictions of *PGA* (top panels) and *PGV* (bottom panels) obtained through eq. (1), EF13, for the Swiss alpine and foreland region, and two empirically based predictive models, namely CH08 and ASB14. Attenuation curves are computed for a scenario M_W 6 strike-slip event (note that only ASB14 allows the explicit introduction of style-of-faulting terms) and $1 \leq R_{RUP} \leq 200$ km. While EF13 is based on R_{RUP}, both ASB14 and CH08 use the distance from the surface projection of the ruptured fault R_{JB} (Joyner & Boore 1981). The empirical models are therefore insensitive to source depth and consequently predict the same ground-motion for events with buried and surface rupture. Such models implicitly assume an average source depth and corresponding near-source saturation. For sake of simplicity, the scenarios shown in Fig. A1 were computed assuming a causative fault with $dip = 90$ degrees and buried at 5 km depth, so that $R_{RUP} = (R^2_{JB} + 5^2)^{1/2}$. ASB14 attenuation refers to $V_{S,30} = 1105$ ms^{-1}, while for CH08 we used the coefficients for generic rock-like ground type. For EF13, the peak-motion variability encompassed by the stochastic simulations is presented in Fig. A1 by displaying the median attenuation curves for $\Delta\sigma$ equal to 10 and 120 bar, along with the 60 bar model recommended by Edwards & Fäh (2013). For the Swiss alpine region, for both *PGA* and *PGV*, ASB14 and CH08 are in good agreement with EF13(60 bar) and EF13(120 bar) models, respectively. At distances shorter than ∼10 km, the *PGA* prediction of CH08 presents a remarkably stronger saturation than EF13. This, at least in part, is due to the choice of distance metric (R_{JB}) and functional form adopted by CH08. In

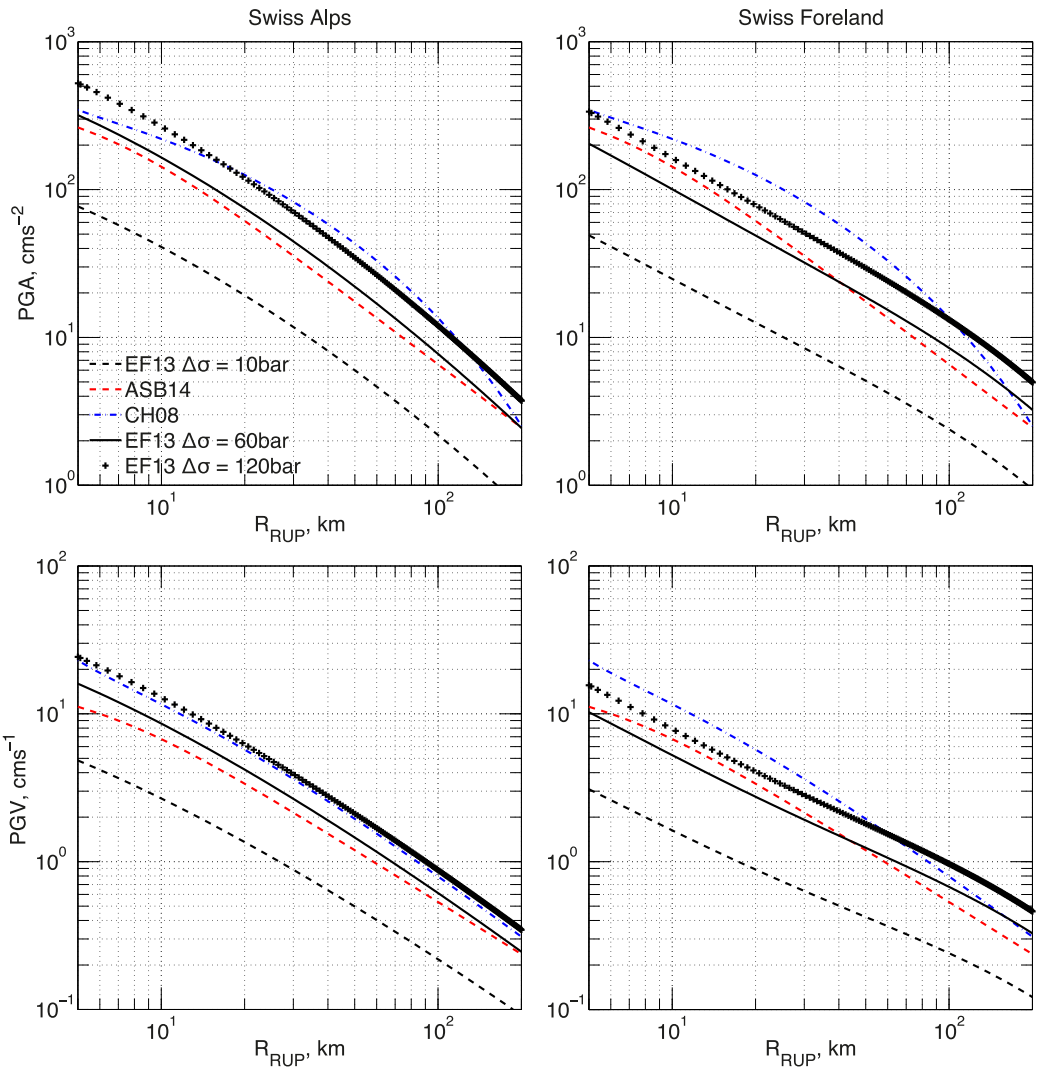

Figure A1. Median predictions of EF13 (10 bar, 60 bar and 120 bar) in the Swiss alpine (left-hand side) and foreland (right-hand side) region compared to ASB14 and CH08, for a scenario M_W 6 strike-slip event, as described in the text. Top panels show *PGA*, while *PGV* is depicted in the bottom panels.

the Swiss Foreland, the empirical and the stochastic models exhibit different rates of attenuation with distance. In terms of overall amplitude, while ASB13 still shows a relatively good agreement with EF13(60 bar), CH08 exceeds EF13(120 bar) over a broad distance range (100 km for *PGA* and 50 km for *PGV)*.

The comparison of EF13 with empirical predictive models at three selected spectral ordinates, $T = 0.3$, 1 and 3 s, consistent with the USGS-*ShakeMap* webpages, are depicted in Fig. A2. CH08 could not be used for this comparison as the model allows only the prediction of *PGA*, *PGV* and low-cut filtered peak ground displacement *PGD*. We use instead the predictive equations of Cauzzi & Faccioli (2008), CF08, in addition to ASB14. The focal distance R to be used with CF08 was computed from R_{RUP} using the empirical equation of Faccioli *et al.* (2010), calibrated on a global databank of shallow crustal earthquakes:

$$R\,(\mathrm{km}) = 2.122 + 0.991\,R_{RUP}\,(\mathrm{km}) + 0.016\mathrm{e}^{0.982M_W}. \qquad \text{(A1)}$$

CF08 is one of the global GMPEs (albeit dominated by Japanese data) adopted in the recently completed EC-funded project SHARE (Seismic Hazard Harmonization in Europe, http://www.share-eu.org/, last accessed 3 November 2014) for active shallow crustal earthquakes in the Pan-European region (Delavaud *et al.* 2012).

The median *PSA* amplitudes in Fig. A2 were computed based on the same scenario as in Fig. A1, i.e. a M_W *6* strike-slip event occurring on a vertical fault buried at 5 km depth, recorded at sites with $V_{S,30} = 1105$ ms^{-1}. In the alpine region, the spectral amplitudes predicted by the empirical models tend to be closer to the lower bound of the median synthetic predictions EF13(10 bar), though there is good agreement in the shape of all attenuation curves. In particular, for *PSA* ($T = 1$ s), CF08 is identical to EF13(10 bar). For the Swiss foreland region, immediately apparent from the plots is the difference in shape between the empirical and the synthetic models, the empirical models exhibit much stronger saturation in the near-source region. The amplitude of the empirical predictions is consistent with the variability encompassed by the stochastic model for different maximum stress-drop values. In general, the empirical and preferred synthetic model EF13(60 bar) show a better agreement for *PGA* and *PGV* than for the selected PSA ordinates.

The median spectral amplitudes predicted by EF13(10 bar), EF13(60 bar) and EF13(120 bar) for a M_W 6 vertical strike-slip event at $R_{RUP} = 10$ km are shown as black curves in Fig. A3. Top panels show 5 per cent-damped *PSA* spectra in the vibration

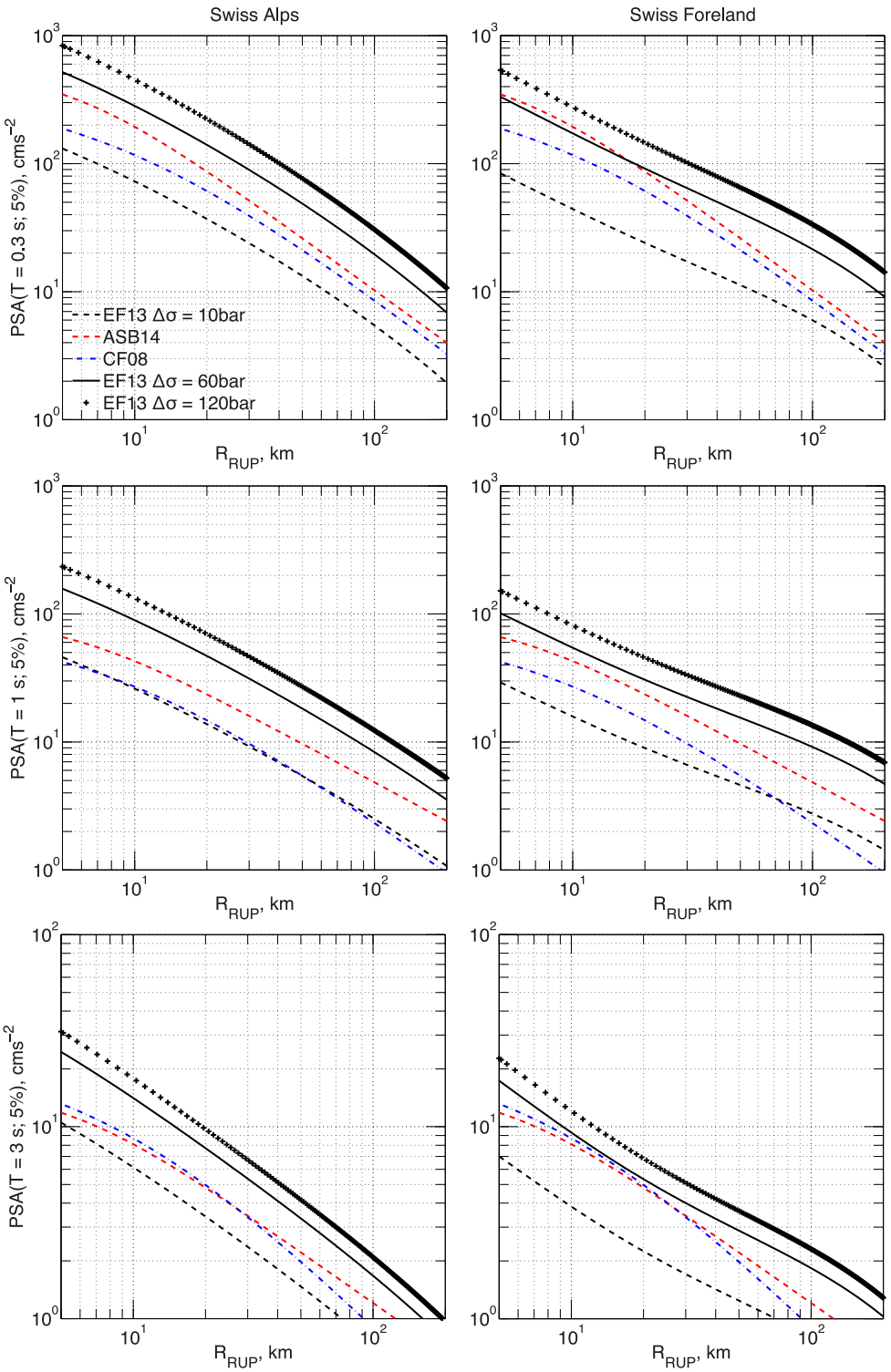

Figure A2. Comparison of median EF13 (10 bar, 60 bar and 120 bar) attenuation curves for the Swiss alpine (left-hand side) and foreland (right-hand side) region with ASB14 and CF08, for a M_W6 strike-slip event, as described in the text. Top panels: *PSA* ($T = 0.3$ s), bottom panels: *PSA* ($T = 3$ s) and mid panels: *PSA* ($T = 1$ s).

period range 0.01 s–4 s, compared with ASB14 predictions (red curves). The 16th percentile spectrum of ASB14 is in good agreement with the median spectral levels predicted by EF13(10 bar) in the alpine region. In the Swiss foreland region, the median prediction of ASB14 are close to the median *PSA* amplitude of EF13(60 bar). The dominant peak of EF13 apparent at vibration periods $T < 0.1$ s is consistent with the well-constrained hard rock reference rock model used in the simulations (Poggi *et al.* 2011). At long periods (bottom panels), where the 5 per cent-damped displacement response spectra *DRS* (T; 5 per cent) can be used for comparison, the 16th percentile amplitudes of CF08 show a relatively good agreement with EF13(10 bar) both in the alpine and foreland region. The synthetic and the empirical model both show a corner period at ∼2 s, although the CF08 spectra for this magnitude and distance

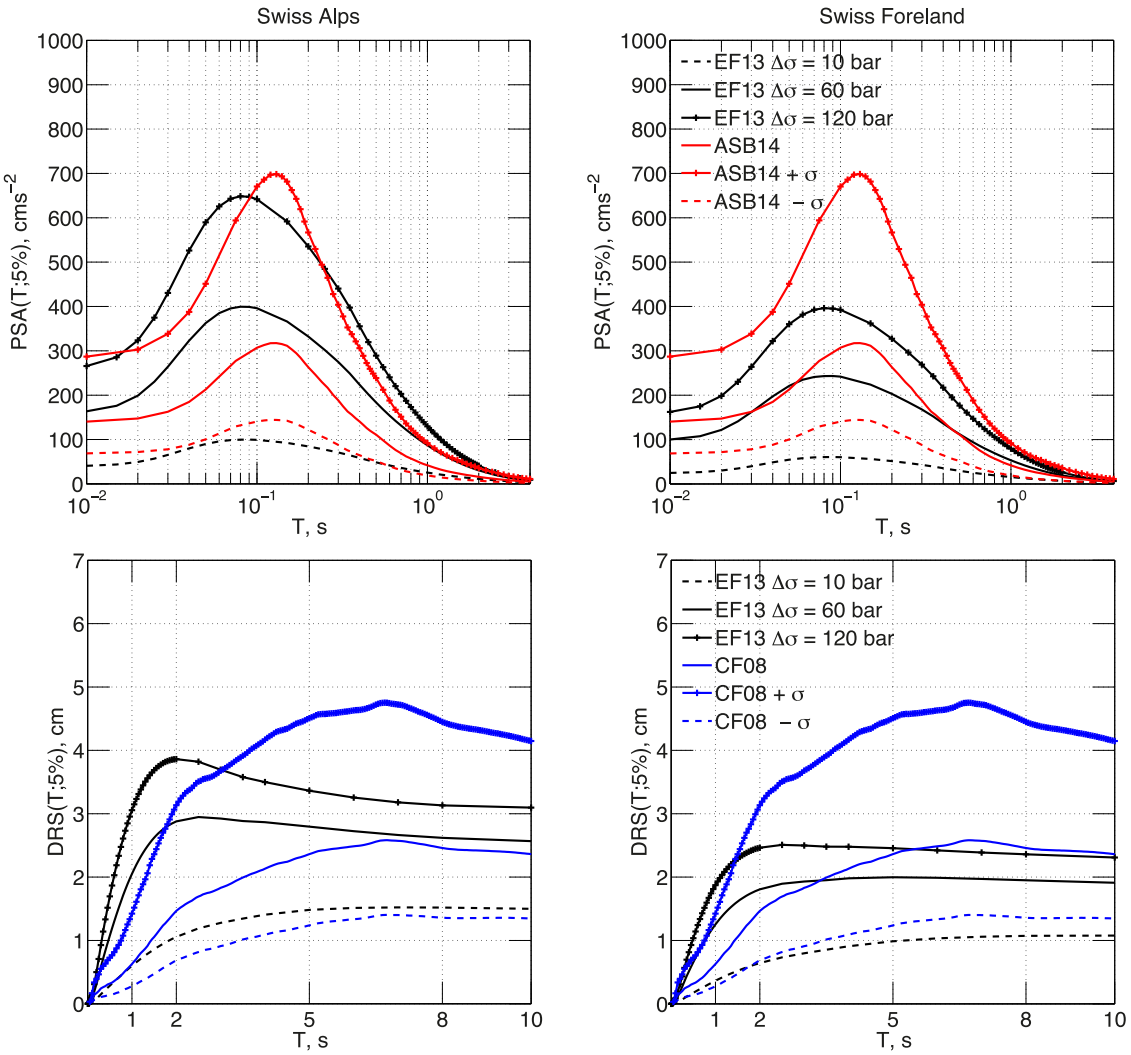

Figure A3. Median *PSA* (*T*; 5 per cent) (top panels) and *DRS* (*T*; 5 per cent) amplitudes (bottom panels) as predicted by EF13(10 bar, 60 bar and 120 bar), ASB14 and CF08, for a M_W6 strike-slip event recorded at 10 km rupture distance, as described in the text.

continue to increase up to ∼7 s before bending gently to approach the peak ground displacement.

SUPPORTING INFORMATION

Additional Supporting Information may be found in the online version of this article:

(http://gji.oxfordjournals.org/lookup/suppl/doi:10.1093/gji/ggu404/-/DC1).

Please note: Oxford University Press is not responsible for the content or functionality of any supporting materials supplied by the authors. Any queries (other than missing material) should be directed to the corresponding author for the article.